ANL-76-128

ANL-76-128

POSTIRRADIATION EXAMINATIONS OF ELEMENT G-3 FROM THE GCFR F-1 SERIES OF MIXED-OXIDE ELEMENTS AFTER ~3 at. % BURNUP

by

R. V. Strain

ARGONNE NATIONAL LABORATORY

ARGONNE NATIONAL LABORATORY, ARGONNE, ILLINOIS

Prepared for the U. S. DEPARTMENT OF ENERGY
under Contract W-31-109-Eng-38

DISCLAIMER

Printed in the United States of America
Available from
National Technical Information Service
U. S. Department of Commerce
5285 Port Royal Road
Springfield, VA 22161

NTIS price codes
Printed copy: A03
Microfiche copy: A01

Distribution Category:
Gas Cooled Reactor Technology
(UC-77)

ANL-76-128

ARGONNE NATIONAL LABORATORY
9700 South Cass Avenue
Argonne, Illinois 60439

POSTIRRADIATION EXAMINATIONS OF ELEMENT G-3 FROM THE GCFR F-1 SERIES OF MIXED-OXIDE ELEMENTS AFTER ~3 at. % BURNUP

by

R. V. Strain

Materials Science Division

February 1977
(Published September 1980)

THIS PAGE

WAS INTENTIONALLY

LEFT BLANK

TABLE OF CONTENTS

LIST OF FIGURES

LIST OF FIGURES

LIST OF TABLES

THIS PAGE

WAS INTENTIONALLY

LEFT BLANK

POSTIRRADIATION EXAMINATIONS OF ELEMENT G-3 FROM THE GCFR F-1 SERIES OF MIXED-OXIDE ELEMENTS AFTER ~3 at. % BURNUP

by

R. V. Strain

ABSTRACT

Postirradiation examinations were performed on element G-3, from the GCFR F-1 series of mixed-oxide elements, after 2.6 at. % burnup in EBR-II. The 20% cold-worked Type 316 stainless steel clad G-3 element was irradiated as an encapsulated element using a stainless steel thermal barrier to achieve peak cladding temperatures of 690°C at a peak power of 14.4 kW/ft. The maximum diametral increase of the element was 0.2% $\Delta D/D_0$. The volatile fission products were found just above the top of the fuel column and in a gap between the bottom and next higher fuel pellet. Annular pellets were used in the element, and at 2.6 at. % burnup, the central hole was closed by fuel material at both the top and the bottom of the fuel column. Fission-product attack of the cladding was minimal; a uniform matrix attack of only 0.3 mil was found along most of the length of the fuel column.

I. INTRODUCTION

The G-3 fuel element was one of 13 elements in the encapsuled F-1 series[1] irradiated in Experimental Breeder Reactor II (EBR-II) by the General Atomic Company (GA) as part of the Gas-Cooled Fast-Breeder Reactor (GCFR) Program. The general objective of the F-1 experiment was to study fuel-element behavior at higher cladding temperatures than obtained in previous LMFBR Program Irradiations. The experiment was designed to produce cladding temperatures as high as 800°C in one element, whereas the remaining elements had temperatures ranging from 600 to 750°C. The design of the experiment also included the use of larger diameter fuel elements, 0.300 in. rather than the 0.230 in. LMFBR elements, that are typical of future GCFR elements. Charcoal traps were placed in some of the elements to obtain data on the behavior of activated charcoal under conditions that may be encountered in the pressure-equalization and gas-purification systems of GCFR plants.

The F-1 experiment is being irradiated in a Mark B-7B subassembly, a seven-capsule array, with planned interim examinations at burnups of approximately 25,000, 50,000, 75,000, and 100,000 MWd/Te. The G-3 capsule was removed

from the subassembly after 25,000 MWd/Te, whereas the other six capsules and a replacement capsule have continued to higher burnup. Initial nondestructive examination of the G-3 capsule was performed at the Hot Fuels and Examination Facility (HFEF) of Argonne National Laboratory at the EBR-II site in Idaho. The disassembly of the capsule and the postirradiation examination of the element were performed in the Alpha-Gamma Hot-Cell Facility (AGHCF) of the Materials Science Division in Illinois.

A. Capsule and Fuel-element Descriptions

The G-3 capsule was composed of three major components: the outer capsule, the thermal barrier, and the element, as shown in Fig. 1. The fuel element consisted of a 13.5-in.-long fuel column with a 0.2595 in. outside diameter (OD) by 0.250-in.-long annular fuel pellets that had 0.059-in. diam central holes. The bottom of the fuel column coincided with the bottom of the EBR-II core and was located 22.625 in. above the bottom of the capsule. The fuel pellets had dished ends with a dish depth of 0.006 in. The composition of the mixed-oxide pellets was 85 wt % UO_2 (93% ^{235}U) and 15 wt % PuO_2. The nominal fuel density was 91% of theoretical and the nominal smeared density was 83%. The fuel-cladding diametral gap was 0.0035 in. The nominal oxygen-to-metal (O/M) ratio of the fuel was 1.98. A 3-in.-long axial blanket consisting of 0.2595 in. OD and 0.250-in.-long solid pellets of natural UO_2 was located at each end of the fuel column. An Inconel* spring was located above the upper blanket to maintain the pellet-stack geometry. A sealed capsule containing activated coconut charcoal was located near the bottom of both the upper and lower gas plenums. The element was clad with a 0.300 in. OD by 0.0185 in. wall, 20% cold-worked, Type 316 stainless steel tube and was ~58 in. long.

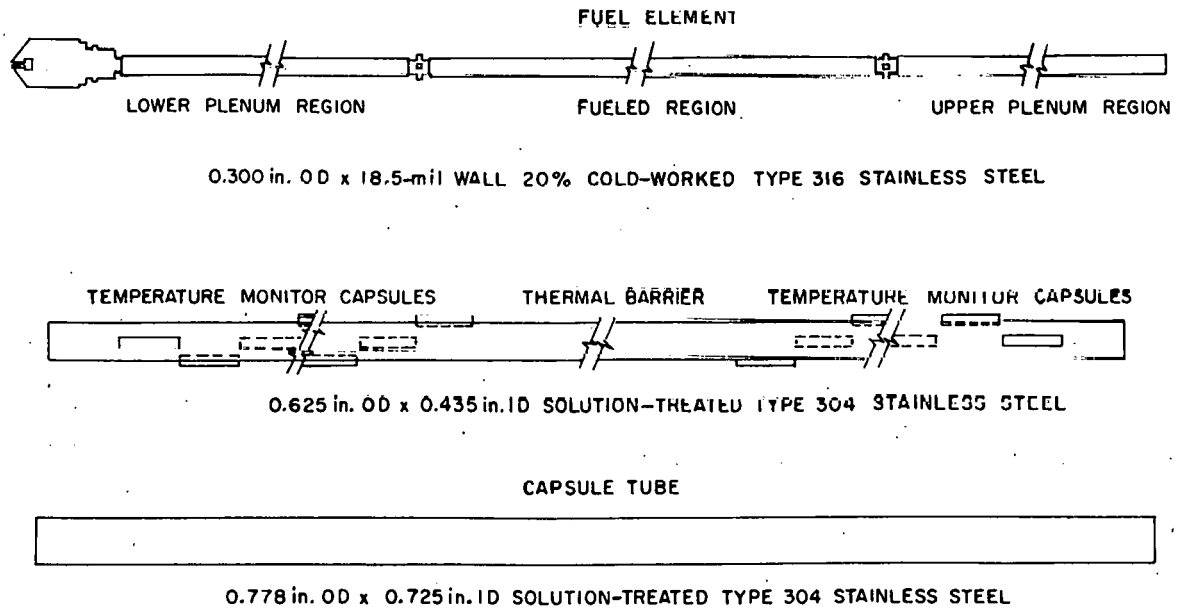

Fig. 1. Major Components of the G-3 Capsule. Neg. No. MSD-166497.

*Trade name for a nickel-base alloy with 70% Ni (min) and 14–17% Cr, 5–9% Fe, and 2-1/4–2-3/4% Ti as the other major constituents.

The thermal barrier consisted of a heavy-walled, solution-treated Type 304 stainless steel tube. The G-3 thermal barrier was ~58 in. long and had a 0.625-in. OD and a 0.435-in. ID. Twenty-four slots, 0.167 in. wide by 0.934 in. long, were cut into the tube to accommodate capsules containing silicon-carbide temperature monitors. Twelve of the monitors were located between 3/4 and 18 in. from the bottom of the barrier, and the remaining twelve were located between 1 and 19 in. from the top of the barrier. A slot ~85 mils wide and 60 mils deep was machined the full length of the barrier to accommodate a dosimeter assembly. The dosimeter assembly consisted of a small capsule (0.042-in. diam) containing 15-mil wires of V, Al, Cu, and small particles of fissile material. Five of these capsules were placed at various axial locations in a 0.065-in. OD by 0.009-in. wall tube running the full length of the thermal barrier.

The outer capsule consisted of 0.778-in. OD by 0.725-in. ID solution-treated, Type 304 stainless steel tube. The overall length of the capsules was 60 in. Heat transfer from the element to the thermal barrier and from the thermal barrier to the capsule was provided by sodium in the annuli. The capsule was wrapped with a 0.020-in.-diam wire to space the capsules and provide mixing of the coolant in the subassembly.

B. Irradiation Conditions

The G-3 capsule was irradiated in position 5 of subassembly X094 in reactor grid position 7B4, which is 11.68 in. from the center of the EBR-II core. The Mark B-7B subassembly is a slightly modified Mark B-7 subassembly with triangular filler strips added to the center of the hexagonal-can flats to reduce the flow area around the outer row of capsules. The size of the capsules was reduced from the standard 0.806-in. OD, for a Mark B-7, to 0.778-in. OD, and a 20-mil-diam spacer wire was added. The reduction of the flow area between the hexagonal can and the outer row of capsules and the coolant mixing that resulted from the spacer wires maintained the overcooling on the periphery of the capsule array at an acceptable level.

The high cladding temperatures achieved in the F-1 experiment were, to a large extent, due to the thermal barrier. The maximum calculated temperature difference of 126°C across the G-3 thermal barrier resulted in a peak cladding temperature of 700 ± 25°C, as shown in Table I. Calculated temperatures for the beginning-of-life capsule, thermal barrier, and element cladding in the core region of capsule G-3 are shown in Fig. 2.

Capsule G-3 was in the EBR-II core from Run 47B through Run 54, but was out of the core for short periods during that span while searches for leaking fuel elements were performed. The total exposure for G-3 was 9113 MWd at 62.5 MW reactor operating power with a maximum total fluence of 2.0×10^{22} nvt. The axial fluence profile is shown in Fig. 3. The fueled portion of the element coincided with the length of the EBR-II core.

TABLE I. Calculated Component Temperatures and Radial Temperature Increases during Peak Power Operation (Run 51A)

Axial Position X/L	Power, kW/ft	Coolant Temperature, °C	Capsule Outer Surface Temperature, °C	Capsule ΔT, °C	Sodium Bond ΔT, °C	Barrier ΔT, °C	Sodium Bond ΔT, °C	Cladding ΔT, °C	Cladding Inside Surface Temperature, °C
Bottom	12.65	372	377	23.2	14.3	115.2	38.3	38.6	607
0.1	12.79	380	386	23.5	14.5	116.5	38.8	38.9	618
0.2	13.31	390	396	24.4	15.1	119.3	40.3	40.4	636
0.3	13.99	401	407	25.7	15.8	124.3	43.6	42.3	659
0.4	14.37	412	418	26.4	16.3	125.7	44.7	43.3	674
0.5	14.42	423	429	26.5	16.3	125.1	44.9	43.4	685
0.6	14.26	433	439	26.2	16.2	122.8	44.4	42.8	691
0.7	13.67	443	449	25.1	15.5	116.8	43.8	40.9	691
0.8	12.97	453	459	23.8	14.7	109.9	41.5	38.7	688
0.9	12.48	463	468	22.9	14.1	104.9	39.9	37.1	687
1.0	12.30	472	478	22.6	13.9	103.4	39.4	36.4	694

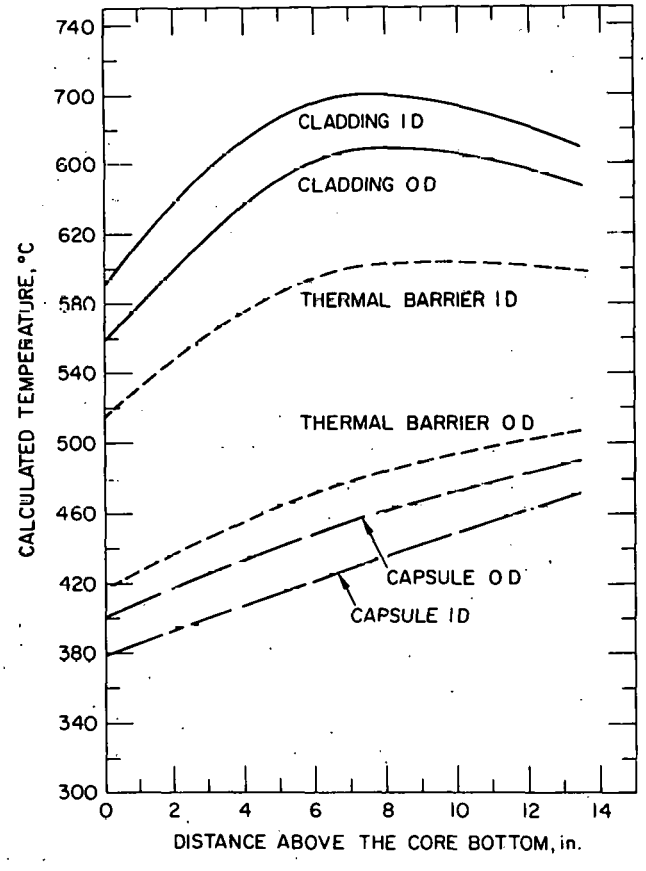

Fig. 2

Axial Temperature Distributions in the Fueled Region of Capsule G-3. Neg. No. MSD-64132.

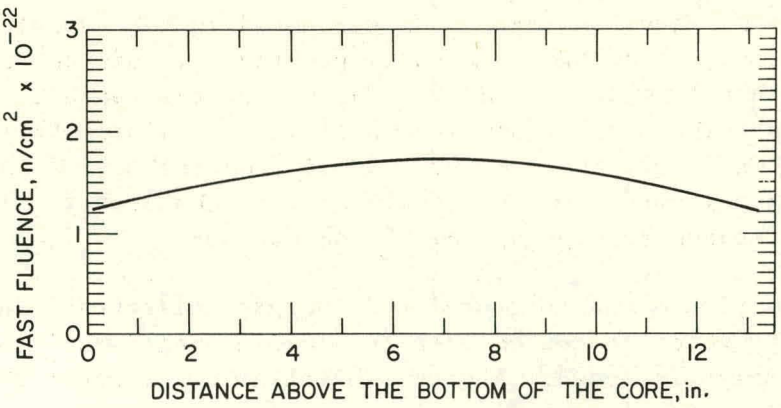

Fig. 3. Fluence Profile for Core Region of Capsule G-3 for Neutrons with Energies >0.1 MeV. Neg. No. MSD-64131.

II. DISASSEMBLY OF THE CAPSULE

The G-3 capsule contained several important components in addition to the fuel element. The retrieval of the temperature monitors and dosimetry capsules resulted in considerable effort being expended in the disassembly of the capsule.

The capsule was examined visually and photographed at a magnification of 0.67X, as shown in Fig. 4. The general condition of the capsule was good. The usual superficial scratches and marks were observed, but no unusual

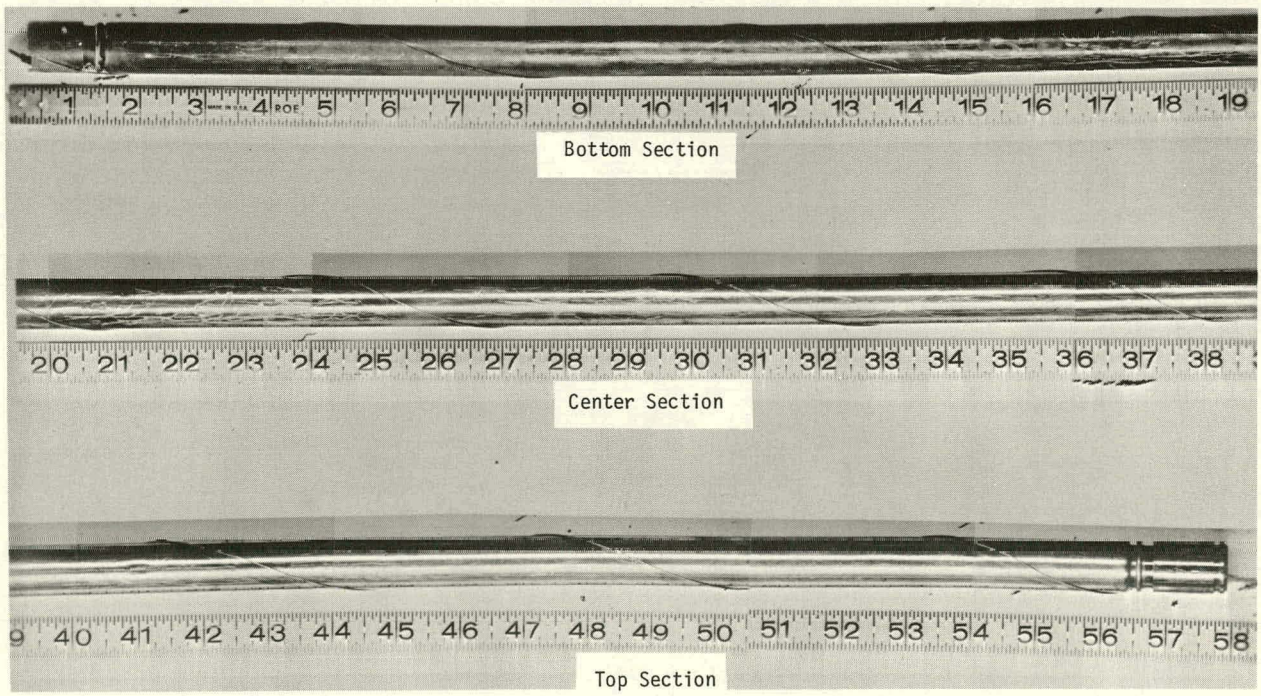

Fig. 4. Macrophotographs of the G-3 Capsule before Disassembly. Ruler was used to accentuate the bow. Neg. No. MSD-181762.

discolorations were seen. A small dent was noted in the capsule ~5 in. from the top. This dent, which had been noted previously,[2] did not occur during shipping to nor handling in the AGHCF. The bow of the capsule was estimated from photographs. The maximum bow was ~0.11 in. at an orientation 35° counterclockwise from the 0° orientation when viewed from the top of the capsule. The direction of bow was away from the center of the subassembly. The maximum bow occurred ~30 in. above the bottom end of the capsule.

The capsule plenum was punctured and the gas collected. The gas exhibited no radioactivity, which indicated that the fuel element was intact, and normal capsule disassembly proceeded. A circumferential cut through the capsule tube was made just above the lower weld. The capsule was heated to ~110°C, and the capsule tube was pulled upward, with respect to the thermal barrier and element, a distance of ~2 in. At this point, no additional separation of the components could be made using the master-slave manipulators. It appeared that the bow in the capsule caused an interference fit between the temperature monitors and the capsule tube, when moved with respect to one another. The initial diametral clearance between these components was 0.005 in. Two additional circumferential cuts were made through the capsule at 20 and 35-1/2 in. from the bottom, and the three sections of capsule tube were removed without additional difficulty. A circumferential cut was made in the thermal barrier just above the lower element weld, the assembly was heated to ~110°C, and the element was easily pulled from the barrier.

The dosimetry assembly (Fig. 5) was removed from the thermal barrier by breaking the tack welds at each end; the tack welds held the assembly in the slot in the barrier. The ~3-in.-long capsules containing the dosimeter wires were removed from the dosimeter tube by means of a thermocouple stripper. The thermocouple stripper (Fig. 6) consisted of a cutting tool mounted in the chuck

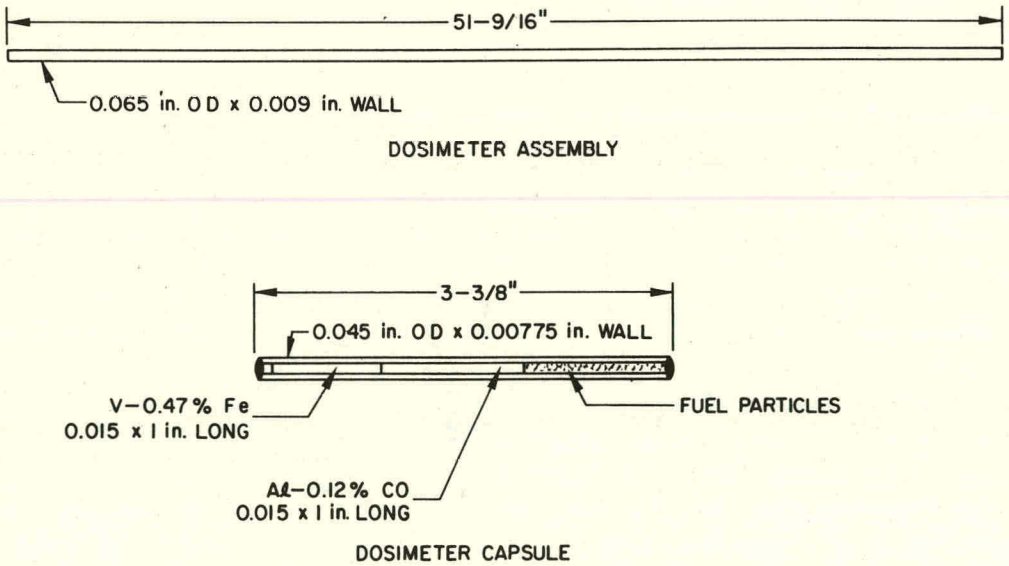

Fig. 5. Dosimeter Assembly from the Thermal Barrier. The assembly contains 10 dosimeter capsules, stainless steel spacers, and a 3-15/16-in.-long tungsten rod. Neg. No. MSD-64133.

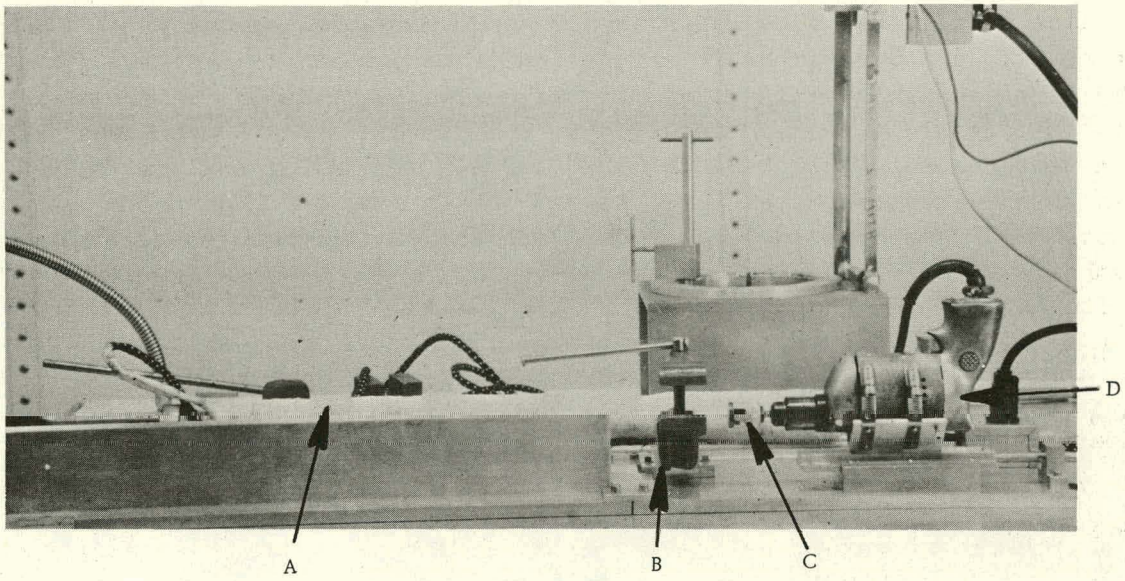

Fig. 6. Thermocouple Stripping Device Used to Deencapsulate the Dosimeters from the F-1 Series of Capsules Irradiated in EBR-II as Part of the GCFR Experiments. A: trough that supports the dosimeter capsule; B: vise used to hold the capsule in position during the stripping operation; C: thermocouple stripping tool; and D: drill motor.

of an electric drill and a trough aligned with the cutting tool. The dosimeter tube was clamped in the trough and the cutter moved so that the dosimeter tube was fed slowly into the cutting tool in increments of ~1 in. The dosimeter tube peeled off in a thin strand as it was fed into the cutting tool. As each of the items in the dosimeter tube was exposed, the stripper was backed off and the item was pulled from the tube. The tube was then fed through the thermocouple stripper until the next item was exposed. The thermocouple stripper made visible scratches on the dosimeter capsules as it peeled off the dosimeter tube, but the scratches were not deep and only extended a short distance (the amount exposed before the capsules were pulled from the tube). The only difficulty encountered during the removal of the dosimetry capsules was that pieces of the strand of tubing from the cutter occasionally clogged the stripper. The dosimeter capsules were shipped to GA for analysis.

A cut-off wheel was used to cut through the tabs of the temperature-monitor capsules to remove the monitors from the thermal barrier. The temperature monitors were numbered consecutively from 1 to 24, starting at the bottom and ending at the top. An attempt was made to remove the Mo capsule containing the temperature monitors from the stainless steel capsules to reduce the radioactivity of the capsules before additional handling. The stainless steel capsules were tapped on a table in an effort to move the Mo capsules to the lower end. The outer capsules were cut as near the upper weld as possible, and the Mo capsules were removed. During this operation, the Mo capsule was opened, and the monitor was found to be contaminated with alpha-bearing material in four of the first twelve capsules. Therefore, no effort was made to remove the other twelve Mo capsules from their stainless steel capsules. All 24 monitors from the thermal barrier were shipped to GA for analysis.

The final step in the disassembly and examination of the capsule hardware was metallographic examination of the braze connection joining a 1/8-in.-diam tube to the capsule-end fitting. This tube was used to inject the bond sodium into the capsule during fabrication of the capsule. The braze was irradiated at a temperature of 370 ± 5°C (700°F) and was exposed to an order of magnitude less fluence than the peak-power region of the capsule. The braze was exposed to the bond sodium at the end of the fill tube inside the capsule. The micrographs in Figs. 7 and 8 show that the braze has not been deleteriously affected by its environment during irradiation.

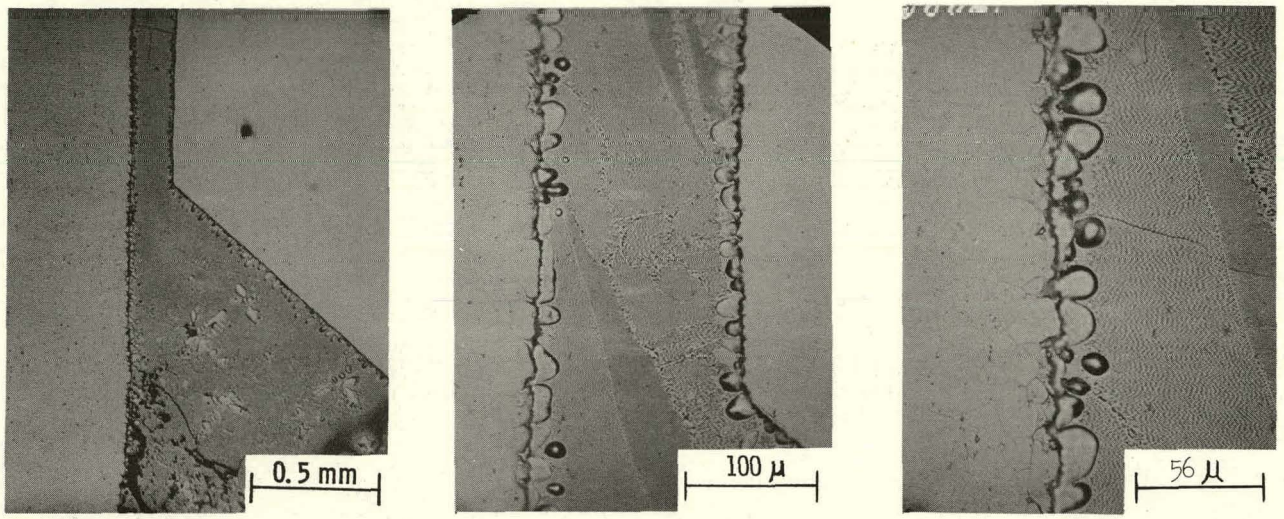

Fig. 7. Microstructure of Sodium Fill-tube Braze and Adjacent Stainless Steel in Archive Sample. Sample was electroetched in 10% oxalic acid. Neg. Nos. (a) MSD-182232; (b) MSD-182234; and (c) MSD-182235.

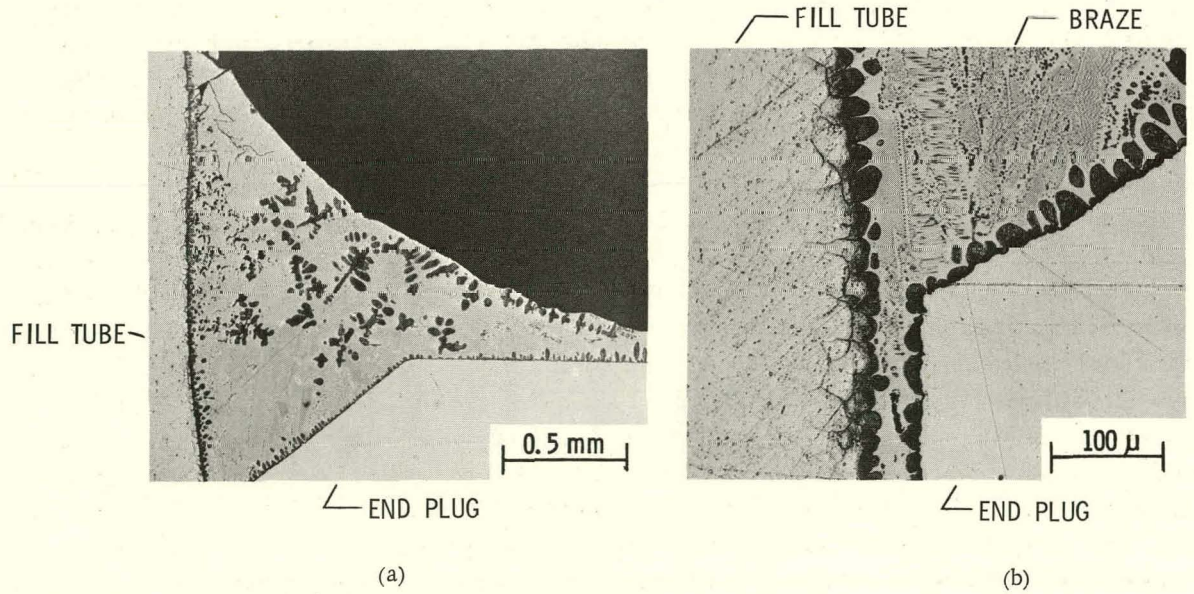

Longitudinal section through the G-3 bottom fill-tube braze after irradiation. Sample was electroetched in 10% oxalic acid.

Fig. 8. Condition of Fill-tube Braze after Irradiation. Neg. Nos. (a) MSD-165597 and (b) MSD-165598.

III. NONDESTRUCTIVE EXAMINATION OF THE ELEMENT

After the element was removed from the thermal barrier, the residual sodium was removed with ethanol and the nondestructive examination was begun. Nondestructive examination consisted of visual examination, gamma scanning, profilometry, and eddy-current scanning.

A. Visual and Photographic Examinations

The visual and photographic examinations of the element showed that its surface was in good condition. The only significant marks on the surface were discolorations between 3 and 17 in. above the bottom weld. These discolorations consisted of two small spots that corresponded to the ends of the monitors in the thermal barrier (Fig. 9). No discolorations were found on the surface of the upper plenum region of the element, although temperature monitors were also placed in this region. The middle section (fueled region) of the element is shown at 0 and 90° orientations in Fig. 10.

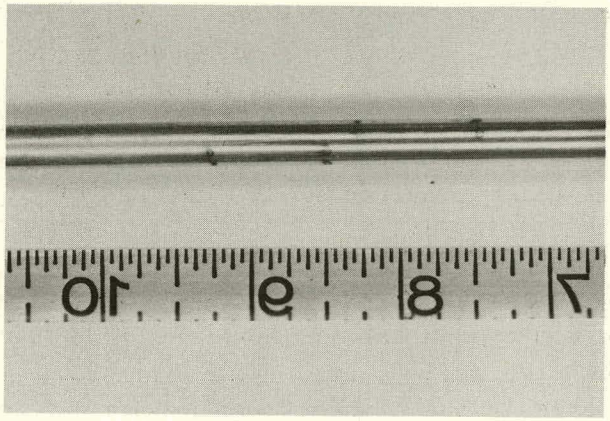

Fig. 9. Discolorations on G-3 Element Cladding 8 in. above the Bottom of the Capsule. The discolorations correspond to the position of the temperature monitors located adjacent to the cladding in the thermal barrier (mirror image). Neg. No. MSD-163773.

The maximum bow of the element, as determined from photographs at a magnification of 1X, was 0.16 ± 0.01 in. at an orientation 120° clockwise from the 0° orientation looking down on the top of the element, or ~180° opposite the bow of the capsule. The maximum bow occurred approximately 30 in. above the bottom of the capsule. The element bow indicates that the element was in interference contact with the thermal barrier at room temperature. However, a bow of this magnitude over the length of the element is not considered severe.

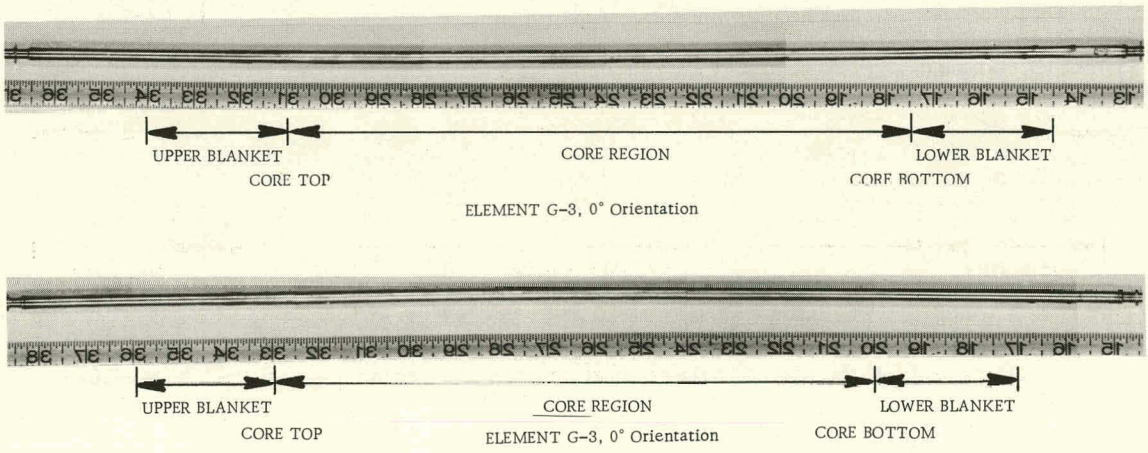

Fig. 10. Fueled Region of the G-3 Element (mirror image). Neg. No. MSD-168571.

B. Gamma Spectroscopy

Gamma spectroscopy was performed on the element with a lithium-drifted germanium (Ge-Li) crystal scintillation detector located external to the AGHCF. During gamma spectroscopy of an element, the gamma rays are collimated through a 4-ft-long collimator with a 1-in.-long variable height (0.01-0.084 in.) slit. The slit opening is covered with a thin aluminum disk to maintain the alpha barrier of the cell. A pulse-height analyzer (4096 channels) and an analog-digital converter are used to convert the signals from the scintillation counter into counts in the energy bands defined by the channels. Each channel represents an energy increment of 50 keV.

Gamma scanning of the element at the AGHCF was initiated on Oct 5, 1972, 218 days after the end of irradiation in EBR-II. Extensive gamma scanning had been performed on the G-3 capsule during the X094 interim examination at the HFEF. However, at that time the activity level of the element was so high that the ^{137}Cs activity could not be distinguished from the background noise. After 218 days of decay time, the ^{137}Cs peak was quite prominent. The results of continuous scans of the element are summarized in Fig. 11. The results of scans for the nonvolatile fission products showed no unusual features except that a gap was apparent between the bottom pellet and the next pellet above. The scan for ^{137}Cs showed a peak near the top of the lower blanket, a sharp peak in the gap between the bottom and the next pellet, and a peak near the bottom of the upper blanket. The ^{137}Cs peaks in the blanket regions are not at the exact fuel-blanket interfaces. The peak in the upper blanket is ~1/4 in. from the interface, and the peak in the lower blanket is ~1/10 in. from the lower interface.

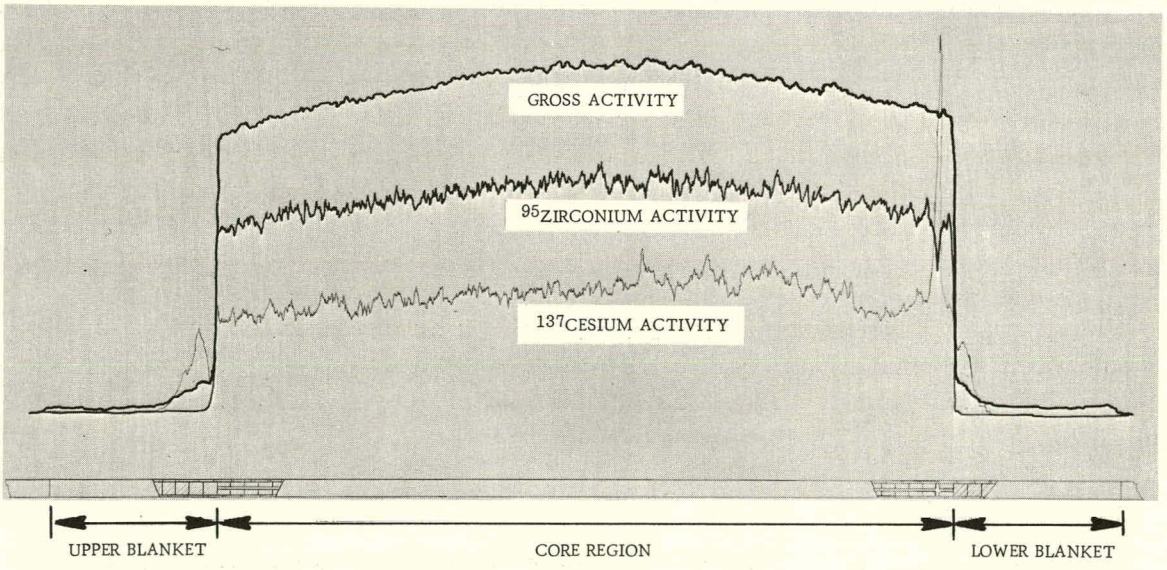

Fig. 11. Continuous Gamma-scanning Results in the Fueled Region of Element G-3. Note the Cs activity peaks at the top and near the bottom of the fuel column. Neg. No. MSD-165629.

C. Profilometry

Diametral measurements were performed on the element using a contact-type profilometer with an accuracy of ±0.0002 in. Measurements were made at orientations of 0, 45, 90, and 135°, and each was checked by duplicating the measurements after the element was rotated 180°.

The results of the profilometry measurements are shown in Figs. 12 and 13. The measured maximum diameter was 0.3008 in. at ~7 in. above the bottom of the core in the 90° orientation. The maximum average (of the four azimuthal orientations measured) diameter was 0.3006 in. The average measured diameter for the upper and lower blanket regions was 0.3003 in. Preirradiation measurements

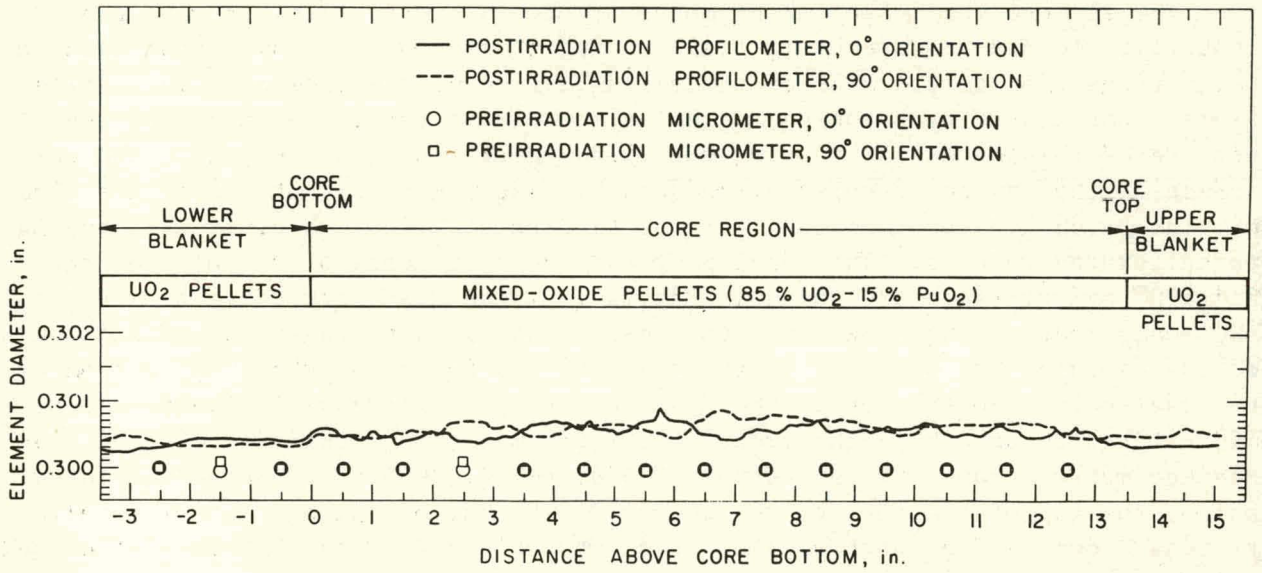

Fig. 12. Results of Diametral Measurements on the G-3 Element at 0 and 90° Azimuthal Orientations. Neg. No. MSD-165630.

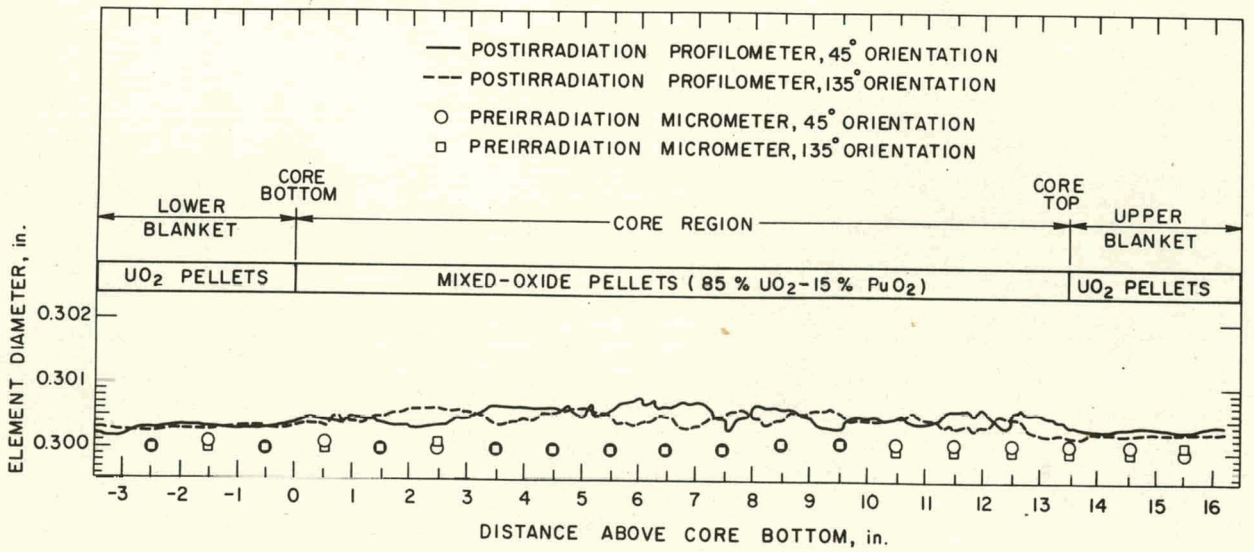

Fig. 13. Results of Diametral Measurements on the G-3 Element at 45 and 135° Azimuthal Orientations. Neg. No. MSD-165663.

of the element were made at ORNL using a micrometer. These measurements showed a fairly uniform diameter of 0.3000 in. over the entire length of the fueled region. The temperature of the element was not measured at the time the post-irradiation diameter measurements were made, but experience with elements at similar burnups indicate that a postirradiation surface temperature of ~75°C could be expected. Therefore, a correction of ~0.2 mil should be subtracted from the postirradiation measurements to account for the thermal expansion of the element cladding. These results indicate a maximum change of 0.2% if the temperature correction is ignored and ~0.13% if the postirradiation measurements are corrected for thermal expansion.

D. Eddy-current Inspection

The element was inspected by means of an eddy-current tester with the capability to detect defects in the cladding ID and OD. The system utilizes a point probe that covers ~18° of the circumference of the element. The entire element was tested by scanning at 15° azimuthal intervals. At present, the results of this method of testing the cladding are qualitative, since the response of the device to defects produced by fission-product attack of the cladding are much greater than the response to discrete flaws machined into tubing as calibrated defects. The results of eddy-current scans of the element at 0 and 180° orientations are shown in Fig. 14. These scans are quite similar to the scans made at the other orientations. These results indicate that attack of the cladding has occurred in the element from 2-1/2 in. above the bottom of the fuel column to the top of the fuel column. The response of the device indicates that attack on the order of several mils has occurred; however, subsequent metallography at the bottom, 3-3/8, 6-7/8, 10-3/4 in. above the bottom, and at the top of the fuel column shows ~0.0003 in. of uniform attack in all regions except at the bottom. No attack was observed at the bottom of the fuel column.

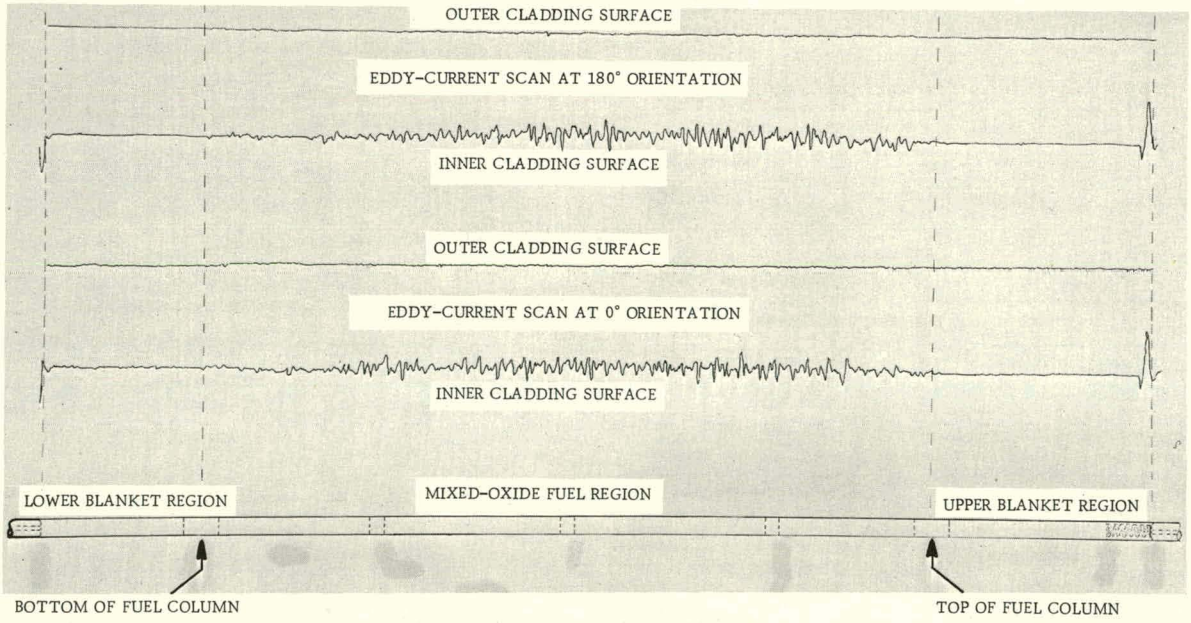

Fig. 14. Results of Eddy-current Testing of the G-3 Cladding after Irradiation. Neg. No.MSD-166499.

IV. DESTRUCTIVE EXAMINATION

Destructive examination of the G-3 element consisted of gas sampling and analyses, flow testing, and ceramographic and metallographic examinations. The testing and sample-preparation procedures as well as the results of these examinations are described.

A. Gas Sampling and Analyses

The gas was removed from the element by drilling into the plenum region, transferring it to an evacuated gas measuring and sampling apparatus, and the pressure was measured in a known volume. These measurements showed that the element contained a total volume of 58.5 ml of gas at STP. The results of mass spectrometry of a sample of this gas are given in Table II. The gas analyses showed a helium content of 33.9% or a volume of 19.8 ml helium at STP. The plenum volume of the element was determined to be 22.1 ml by back filling the element with the cell atmosphere and repeating the gas-volume measuring operation. The discrepancy between the helium volume and the volume of the element plenum could arise from seal welding in a negative pressure glovebox and at an elevated temperature in the vicinity of the weld.

TABLE II. G-3 Gas Analyses

A. Gas Composition

Gas	Volume, %	Volume at STP, ml	Gas	Volume, %	Volume at STP, ml
H_2	<0.1	<0.06	A	0.2	0.12
He	33.9	19.8	CO_2	<0.1	<0.06
H_2, CO	0.09	0.05	Kr	9.2	5.3
O_2	0.01	0.006	Xe	56.5	33.1

B. Isotopic Analyses

Isotope	Volume, %	Isotope	Volume, %
^{83}Kr	15.0	^{131}Xe	15.2
^{84}Kr	26.9	^{132}Xe	22.4
^{85}Kr	6.7	^{134}Xe	34.2
^{86}Kr	51.4	^{136}Xe	28.2

The 5.3 ml of Kr and 33.1 ml of Xe found in the element represent a gas release of ~64%. This release is based on a generation of 0.2055 ml of fission gas per gram of fuel, $(U,Pu)O_2$, per percent burnup. The average burnup for G-3 was estimated as 2.6%. The release of 64% of the fission gas is in good agreement with other data from oxide elements with similar fuel densities and power ratings.

B. Flow Tests

Helium was permitted to flow through several regions of the element to determine whether blockages had occurred during irradiation. The apparatus shown in Fig. 15 was used to measure the differential pressure and flow of helium introduced into the element through small holes drilled in the cladding. The regions of the element that were tested and the entrance and exit points for the gas are listed in Table III. The results of the flow tests, given in Table IV, show that, at room temperature, a relatively free gas flow was evident in the element, except at the ends of the fuel column. The top and bottom fuel-blanket interface regions permitted a helium flow of only 0.3 ml/sec at a differential pressure of ~50 in. of water.

C. Ceramographic and Metallographic Examinations

The ceramographic and metallographic examinations of samples cut from the element constituted a major portion of the destructive examination. These examinations entailed sectioning the element, preparing samples, and performing optical microscopy and electron-microprobe analyses of the fuel and cladding. The element was cut into specimens (Fig. 16), using a slow-speed silicon carbide cutoff wheel. Three transverse and two longitudinal sections were placed in electrically conducting mounts and prepared for optical microscopy and electron-microprobe analyses. During the sectioning operation, specimens were also cut for burnup analyses (temperature determination using the release of ^{85}Kr from the recoil layer of the cladding) and biaxial stress-rupture tests. The experimental determination of the cladding temperature was performed at GA; the results are not included in the present report.

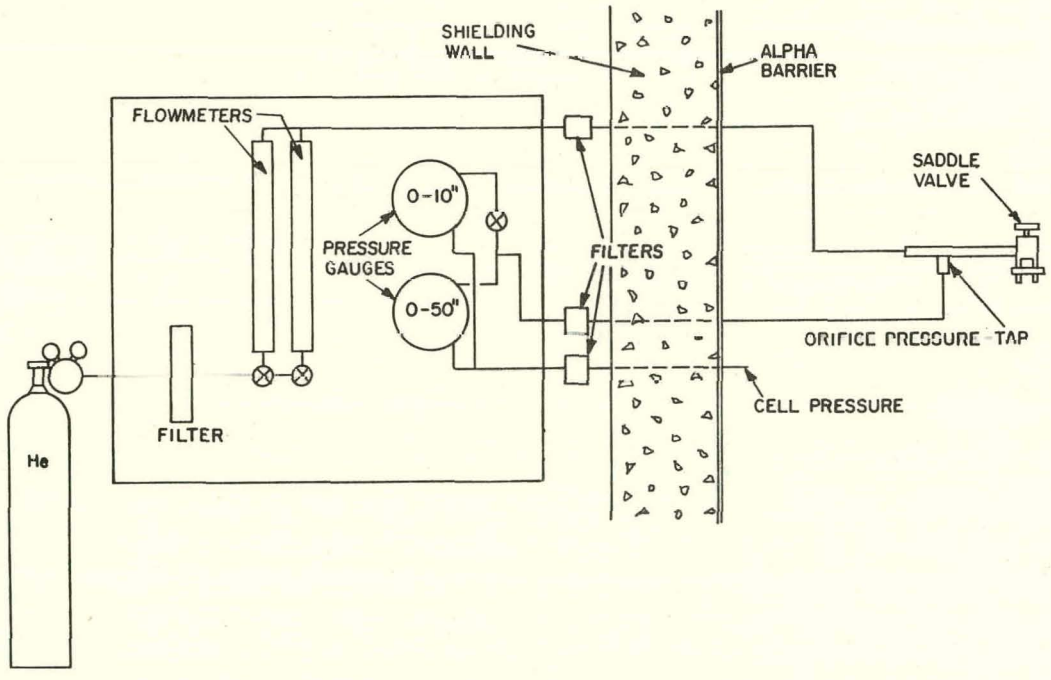

Fig. 15. Flow-testing Apparatus Used to Determine Helium Flow Rates through Several Axial Regions of G-3. Neg. No. MSD-63996.

TABLE III. Gas Flow Paths for G-3 Flow Test[a]

Test Number	Location	Gas In	Gas Out
1	Plenum and Charcoal Trap Region	~23-1/2 in. above reference point	~36-7/8 in. above reference point
2	Blanket Region	~18-3/8 in. above reference point	23-1/2 and 36-7/8 in. above reference point
3	Top Fuel-blanket Interface	~17-5/8 in. above reference point	18-3/8, 23-1/2, and 36-7/8 in. above reference point
4	Fuel Column	9-1/2 in. above reference point	17-5/8, 18-3/8, 23-1/2 and 36-7/8 in. above reference point
5	Bottom Fuel-blanket Interface	4-1/8 in. above reference point	9-1/2, 17-5/8, 18-3/8, 23-1/2, and 36-7/8 in. above reference point

[a]Reference point is located 17.265 in. above the bottom of the element, including the end fitting.

TABLE IV. Results of G-3 Flow Tests

Test Number	Location	Pressure, in H_2O	Flow Rate, ml/s
1	Plenum and Charcoal-trap Region	2	3.0
		4	6.6
		6	9.7
		8	12.5
		10	15.3
		20	28.3
		30	39.8
2	Blanket Region	1.3	0.3
		10.5	1.6
		28.2	4.5
		41.8	6.7
		49.0	8.0
3	Top Fuel-blanket Interface	11.7	0.2
		50	0.3
4	Fuel Column via Central Hole	0.1	0.3
		0.3	1.7
		0.7	4.7
		1.3	9.8
		2.4	17.3
		3.7	25.3
		5.5	33.8
		7.4	42.1
5	Bottom Fuel-blanket Interface	12	0.2
		48	0.3

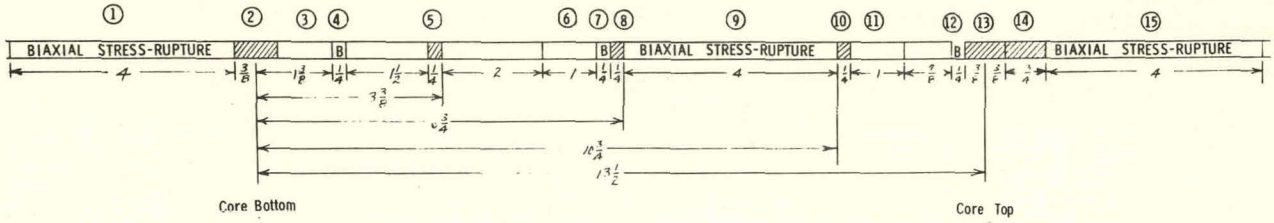

1 Lower blanket biaxial stress-rupture specimen
2 Bottom longitudinal metallographic sample
3 Bottom ^{85}Kr temperature determination specimen
4 Bottom burnup determination specimen
5 Bottom transverse metallographic sample
6 Middle ^{85}Kr temperature determination specimen
7 Middle burnup determination specimen
8 Middle transverse metallographic specimen
9 Fuel region biaxial stress-rupture specimen
10 Top transverse metallographic sample
11 Top ^{85}Kr temperature determination specimen
12 Top burnup determination specimen
13 Top longitudinal metallographic sample
14 Upper blanket longitudinal metallographic sample
15 Upper blanket biaxial stress-rupture specimen

Fig. 16. Cutting Diagram for the G-3 Element. Neg. No. MSD-166495.

The samples for microscopy were prepared in the Materials Science Division's AGHCF using Buehler slow-speed grinding and polishing machines with Whirlimet attachments. The samples were ground using 320- and 600-grit silicon carbide papers and were polished using 3 and 1 μm diamond paste. Hyprez* was used as the coolant in the grinding and polishing steps. The samples were cleaned between preparation steps in ultrasonic baths containing ethanol. The cladding was electrolytically etched using 5% HCl in methanol at 10 V. The hot-cell atmosphere was nitrogen that contained <100 ppm oxygen and ~50 ppm water.

Microscopy of the samples included a series of examinations in the following sequence:

1. Optical microscopy in the as-polished condition was performed on all samples. This included making a composite of each section at a magnification of 50X, photo- graphing areas of interest at magnifications of 250 and 500X, photographing regions of the fuel under polarized light, and determining the radial porosity distribution of the fuel.

2. Electron-microprobe analyses were performed on the bottom longitudinal section, the middle transverse section, and the top longitudinal section. These examinations included attempts to determine the radial distribution of U, Pu, Cs, I, and Te, the composition of selected fission-product inclusions, the composition of the fuel phase adjacent to the cladding, and the composition of the cladding where fission-product attack has occurred.

3. Optical microscopy of the cladding after it was etched.

4. Microhardness measurements on the cladding.

*Hyprez is a trade name for a kerosene-base liquid that does not react with alkali metals.

D. Results of Ceramographic Examination

The as-polished longitudinal and transverse sections of the element are shown as composite photographs in Figs. 17 through 21. These sections show that the fuel has restructured to produce the usual three radial zones, the columnar-grain zone, the equiaxed-grain zone, and the unrestructured zone. The dimensions of the zones are given in Table V. The most striking result revealed in the composites was the closing of the central hole (the fuel was fabricated with a 0.059-in.-diam central hole) near the top and bottom fuel-blanket interfaces. The fuel has also expanded to close the original 0.0035-in. diametral gap between the fuel and the cladding and is essentially in contact with the cladding over the entire length of the fuel column.

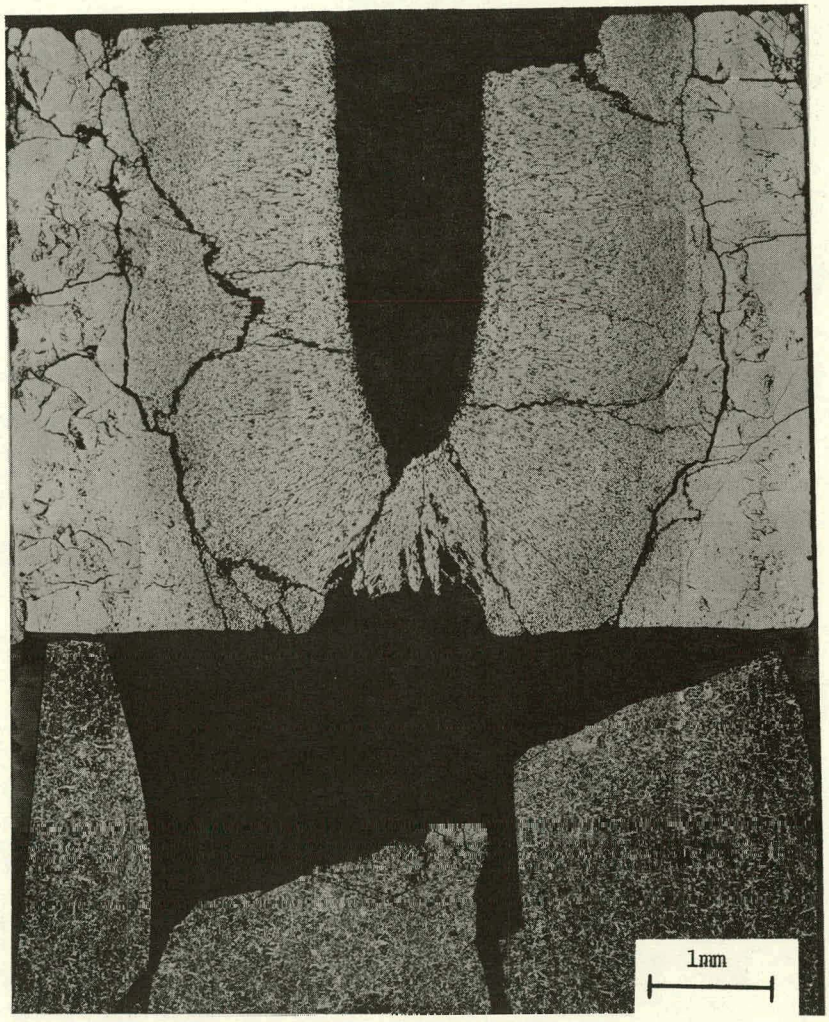

Fig. 17. Composite of the Bottom Longitudinal Section of the G-3 Fuel Column in the As-polished Condition. Neg. No. MSD-165604.

Fig. 18. Composite of the Transverse Section 3-3/8 in. above the Bottom of the G-3 Fuel Column in the As-polished Condition. Neg. No. MSD-165606.

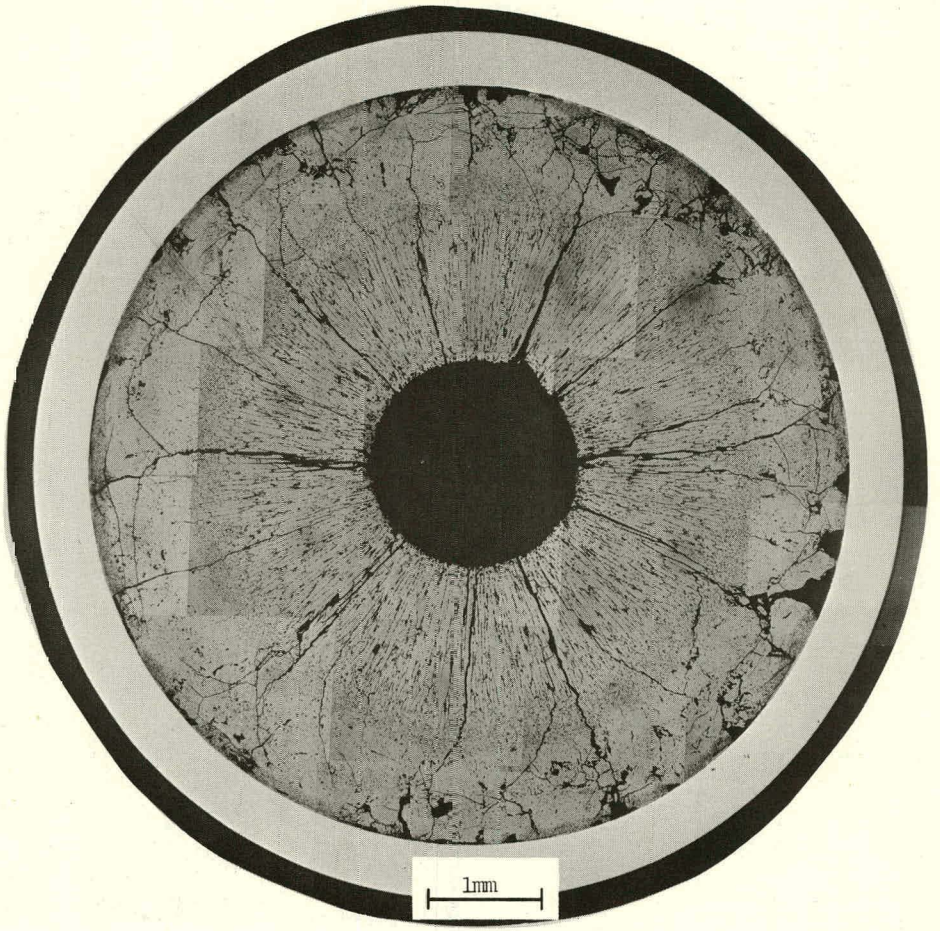

Fig. 19. Composite of the Transverse Section 6-7/8 in. above the Bottom of the G-3 Fuel Column in the As-polished Condition. Neg. No. MSD-165607.

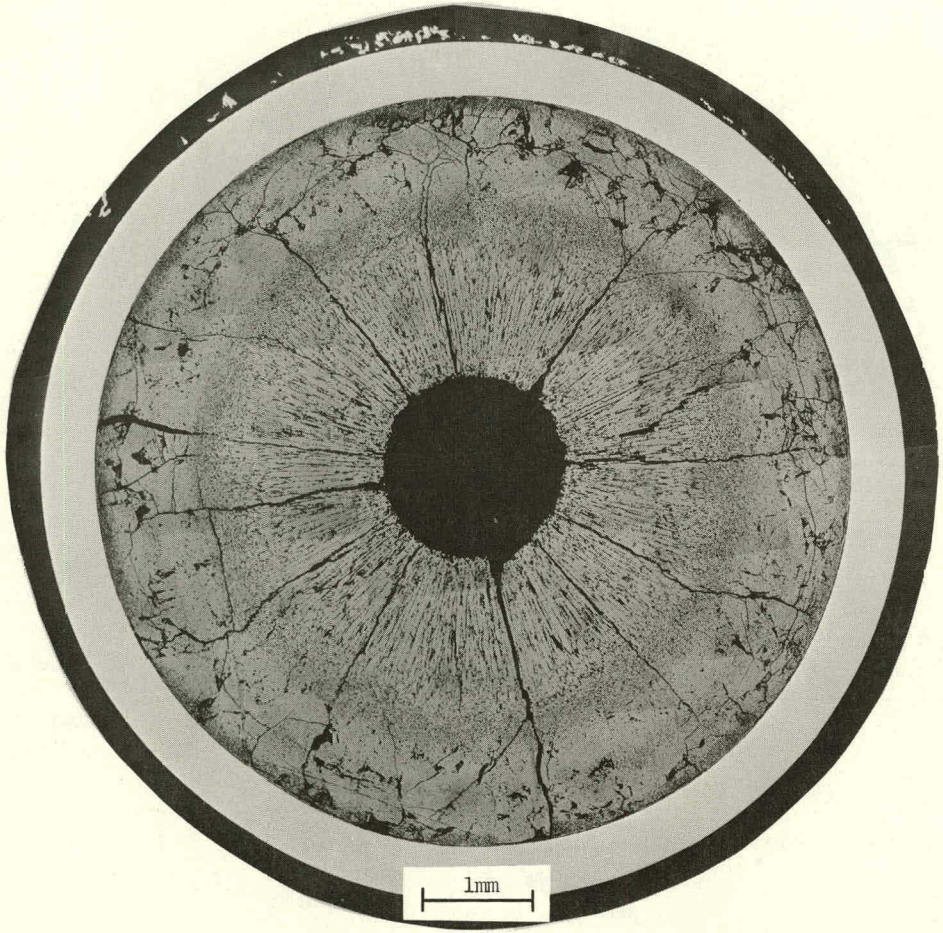

Fig. 20. Composite of the Transverse Section 10-3/4 in. above the Bottom of the G-3 Fuel Column in the As-polished Condition. Neg. No. MSD-165605.

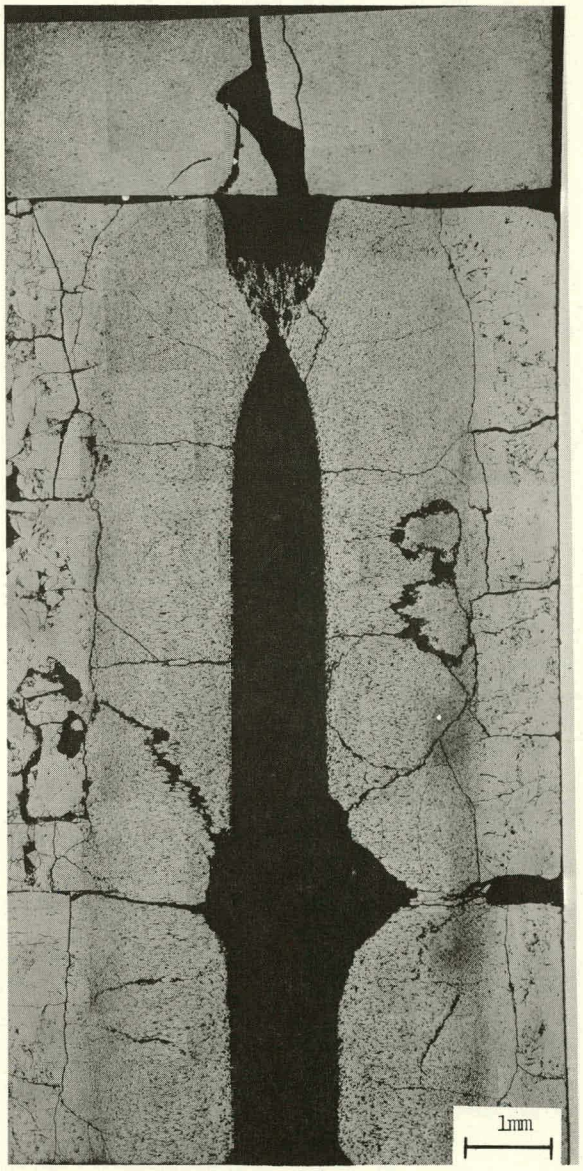

Fig. 21. Composite of the Top Longitudinal Section of the G-3 Fuel Column in the As-polished Condition. Neg. No. MSD-165601.

TABLE V. Metallographic Data for Element G-3

Sample Number	Sample Type	Axial Position,[a] in.	Cladding ID Temperature, °C	Diameter of Central Hole, mils	Diameter of Columnar-grain Zone, in.	Diameter of Equiaxed-grain Zone, in.
91A-5	Longitudinal	Bottom	590	49 max Closed, min[b]	0.140	0.189
91A-9	Transverse	3-3/8	665	64 max	0.177	0.197
91A-13	Transverse	6-7/8	700	72 max	0.183	0.201
91A-15	Transverse	10-3/4	690	63 max	0.173	0.195
91A-19	Longitudinal	13-1/2	670	49 max Closed, min[b]	0.141	0.183

[a]Distance above the bottom of the core.
[b]The central hole appeared to have been closed by fuel-vapor deposition near the fuel-blanket interface.

Metallic fission-product inclusions were distributed throughout the columnar- and equiaxed-grain zones. These fission-product inclusions were relatively few in number and were so small in size that their composition could not be determined with the shielded microprobe.

The typical microstructure of the three zones in the fuel at the reactor midplane are shown in Figs. 22-24. These figures show an area from each of the three zones in the as-polished condition under polarized light and normal incident light. The individual grains are apparent in the photographs made with polarized light but not in those taken with normal illumination. The variations in grain size from quite small grains in the unrestructured zone to the large elongated grains in the columnar-grain zone are evident.

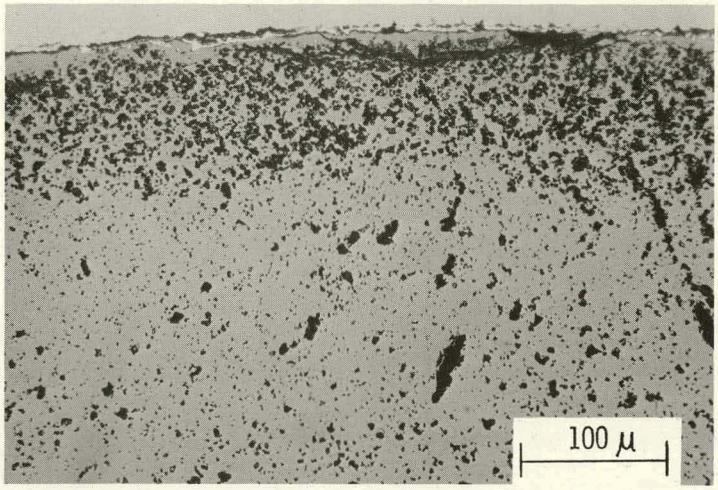

(a)

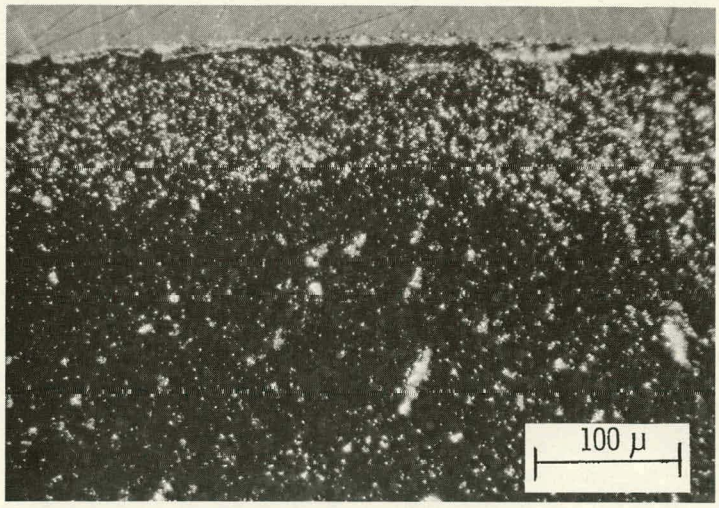

(b)

Fig. 22. Outer Edge of Fuel at the Midlength of the Fuel Column of Element G-3. This area is typical of the unrestructured zone of the fuel. The sample was in the as-polished condition. (a) Normal bright-field Illumination. Neg. No. MSD-164920; (b) Polarized-light Illumination. Neg. No. MSD-164921.

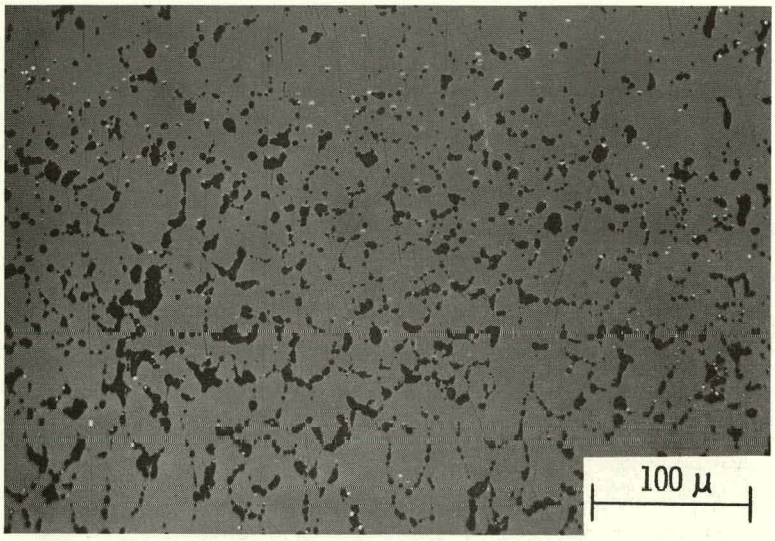

(a)

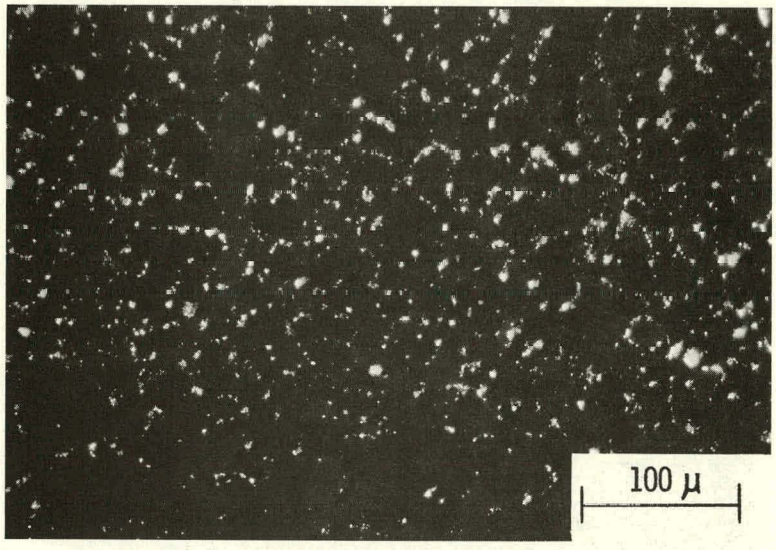

(b)

Fig. 23. Typical Area of Equiaxed Zone at the Midlength of the Fuel Column of Element G-3. The sample was in the "as-polished" condition. (a) Normal Bright-field Illumination. Neg. No. MSD-164922; (b) Polarized-light Illumination. Neg. No. MSD-164923.

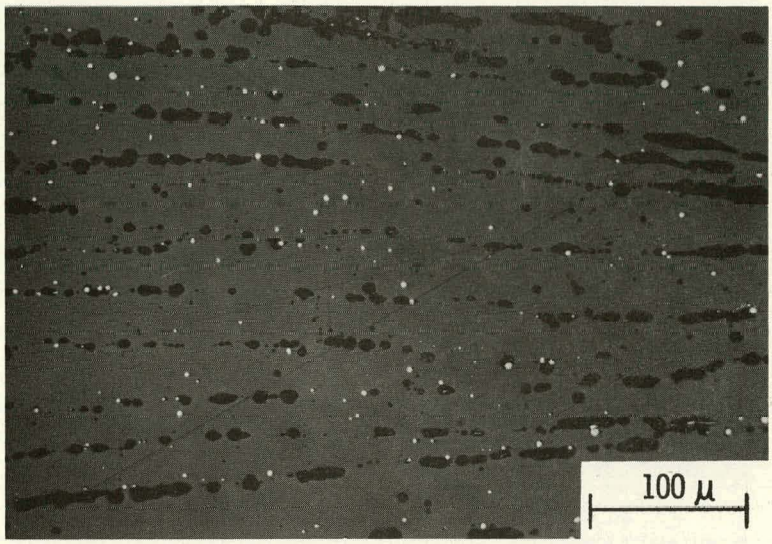

(a)

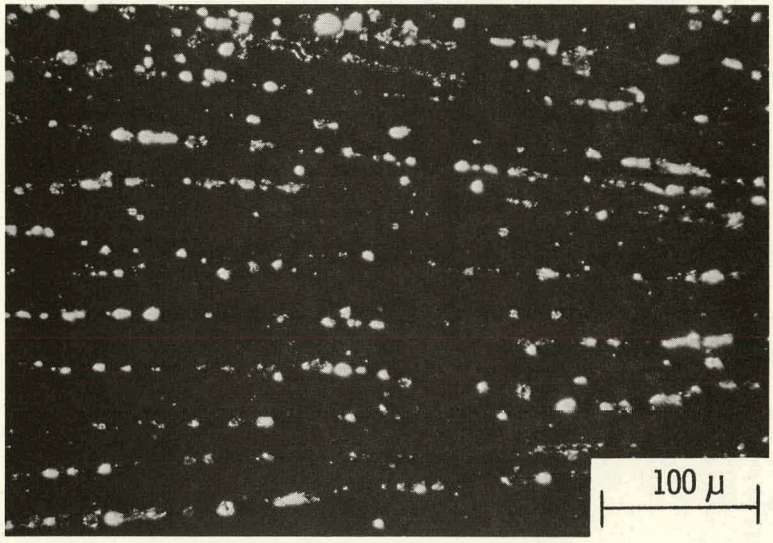

(b)

Fig. 24. Typical area of the Columnar-grain Zone at the Midlength of the Fuel Column of Element G-3. The sample was in the "as-polished" condition. (a) Normal Bright-field Illumination. Neg. No. MSD-164924; (b) Polarized-light Illumination. Neg. No. MSD-164925.

E. Fuel-density Determination

The density of the fuel in the metallographic sections was determined using a Quantimet image analyzer. The measurements were made by projecting an image of the fuel microstructure on a vidicon scanner. Features in the microstructure can then be detected according to their gray level. The threshold of detection is selected by the operator and the area corresponding to that gray level is calculated by the computer portion of the system.

The Quantimet measurements of the void area have an error of ±2% as determined by calibrating the instrument with UO_2 specimens of known density at a magnification of 250X. The main source of error in the measurement was the result of operator judgment being required to set the threshold of detection, which in turn, affected the detected void size. The threshold of detection did not change during a traverse across the fuel radius. Therefore, the measurement of the relative density across a specimen was more accurate than the measurement of density from specimen to specimen. Other factors affecting the accuracy of the measurement were the extent of fuel pullout during sample preparation and the presence of large cracks in the fuel. Both of these errors were difficult to quantify, but they could be minimized by careful selection of the radii to be traversed and careful sample preparation. It should be noted that both of these errors tend to make the measured density less than the actual density.

The percent of fuel density, measured at a magnification of 200X for the G-3 sections is shown in Figs. 25-27. The densities shown for the transverse sections are the average of two radial traverses. The traverses were selected as those representative of the general fuel structure. Large cracks and any areas of fuel pullout were avoided. The fuel densities for the longitudinal

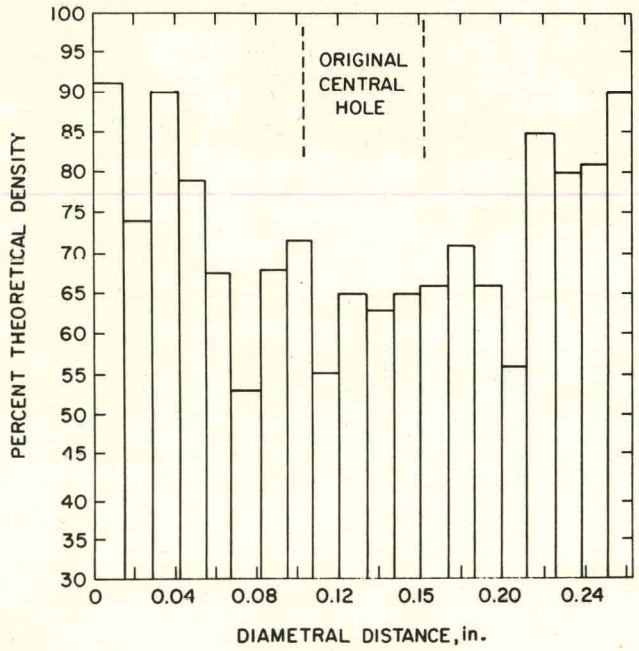

Fig. 25

Diametral Distribution of Fuel Density for the Bottom Longitudinal Section from Element G-3. The determinations were made along a line through the region where the central void has been closed. Neg. No. MSD-64129.

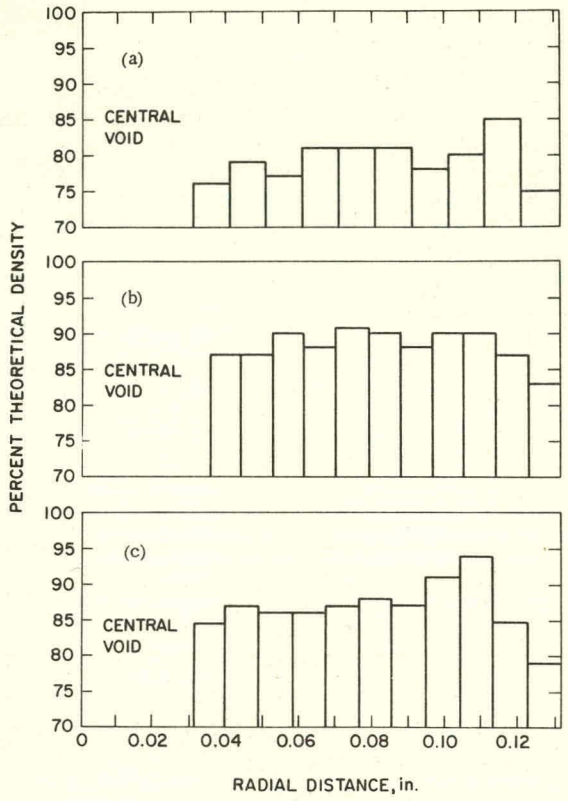

Fig. 26. Radial Distribution of Fuel Density in the Transverse Sections from G-3. (a) Section 10-3/4 in. above core bottom; (b) Section at the core mid-plane; (c) Section 3-3/8 in. above core bottom. Neg. No. MSD-64128.

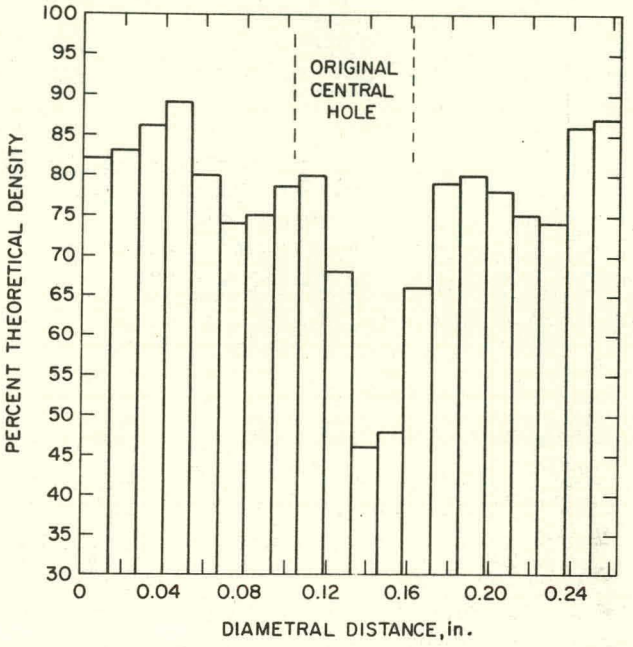

Fig. 27. Diametral Distribution of Fuel Density for the Top Longitudinal Section from Element G-3. The determinations were made along a line through the region where the central void has been closed. Neg. No. MSD-64130.

sections were obtained from a single diametral traverse across the fuel at the fuel bridge near the ends of the fuel column. Since cracks in the fuel could not be avoided during these traverses, low-density values (55%) appear in the density distributions. The cracks are particularly evident for the bottom longitudinal section.

The generally low-density values for the 10-3/4-in. section, when compared with the other sections, are substantiated by a qualitative indication of greater porosity on the composite photograph at a magnification of 40X. The lower density may reflect the lower power rating in this region or a pellet-to-pellet variation in the as-fabricated density. Otherwise, these density distribution results showed no unusual trends.

F. Burnup Determination

Based on interpolation between measured values, the peak burnup of the element was ~2.8 at. %. Burnup determinations were made with both ^{140}Nd and ^{139}La as the burnup monitors. The Nd and La internal spikes were added to the same aliquot and run simultaneously on the mass spectrometer. The burnup values reported by Ebersole[3] for both monitors are given in Table VI.

TABLE VI. Burnup Determinations

Sample Number	Distance above Core Bottom, in.	Measured Burnup, at. %	
		$^{148}Nd^{a}$	$^{139}La^{b}$
91A-7	1.5	2.26	2.28
91A-12	6.4	2.61	2.67
91A-18	13.0	2.14	2.12

[a]Nd fission yields for ^{235}U and ^{239}Pu were 1.63 and 1.70, respectively.
[b]La fission yields for ^{235}U and ^{239}Pu were 6.30 and 5.8, respectively.

G. Electron-microprobe Analyses of the Fuel

Electron-microprobe examinations were performed on three sections of the fuel (the transverse section from the reactor midplane and the top and bottom longitudinal sections). Attempts were made to determine the distribution of the volatile fission products Cs, Te, and I in these sections. The quantities of these fission products in the bottom and midplane sections were below the detection limits of the shielded microprobe. In the top longitudinal section, a small quantity of Cs was detected in the gap between the fuel and cladding. Tellurium and iodine were not detected.

The radial distribution of Pu in the fuel was determined by point counting at ~0.01-in. intervals from the central void to the outer edge. For each section, the high density fuel near the central void was used as an internal standard. The maximum counting deviations were 1.8 and 0.8% for Pu and U, respectively, in this "standard." Relative concentrations of Pu and U were calculated from the ratio of the net counting rate at each location to the average for the respective standards. These relative concentrations were then normalized by assuming a fuel composition of 15 wt % PuO_2-85 wt % UO_2 in the unrestructured zone.

The Pu distribution results for the top, bottom, and midplane of G-3 are shown in Figs. 28-30. The radial traverses across the fuel pellets (circles in the figures) indicate a segregation of Pu toward the central void which results in fuel containing ~19 wt % PuO_2 adjacent to the central void. The mid to outer region of the columnar-grain zone and the inner half of the equiaxed-grain zone were slightly depleted in Pu as a result of actinide redistribution. The actinide distribution in the material that was transported to the central hole at the top and bottom of the fuel column during irradiation was also determined. These results (triangles in the figures) show that the material filling the central hole at the bottom of the fuel column had a distribution (Pu content versus distance from the central void) quite similar to the radial distribution of the pellets. The Pu content in the fuel filling the central void at the top of the fuel column was depleted in Pu, particularly near the inner edges of the deposited fuel, which is the reverse of that observed in the pellets.

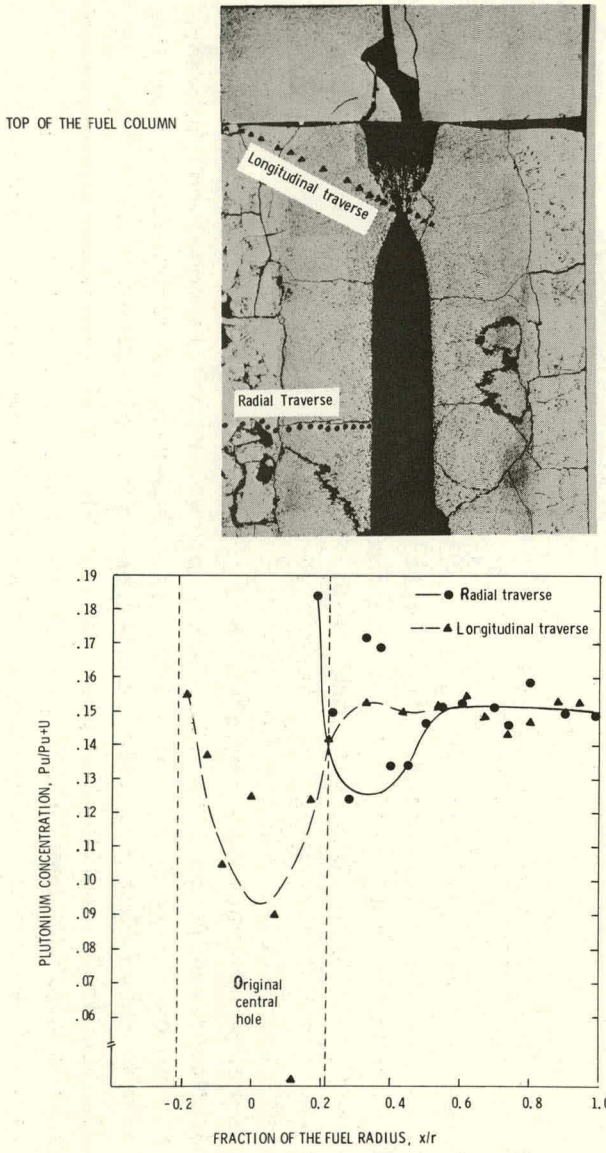

Fig. 28. The Pu Distribution Near the Top of the Fuel Column in Element G-3. Neg. No. MSD-180623.

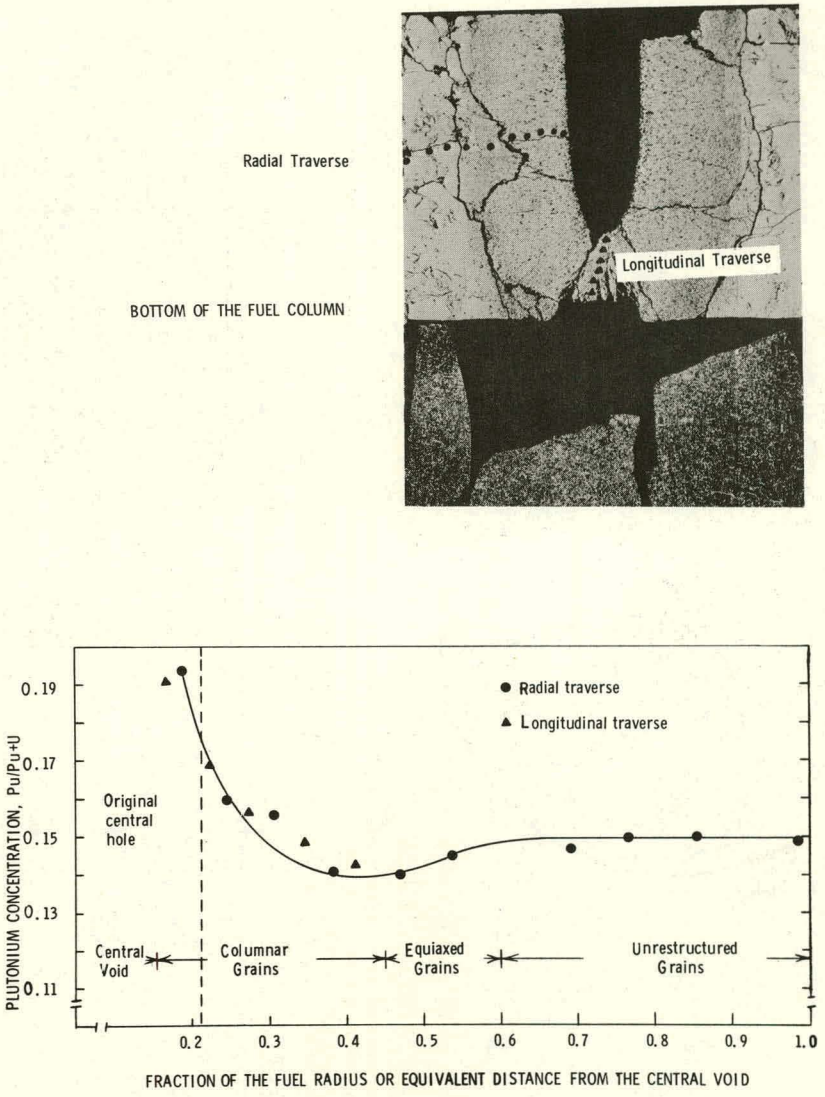

Fig. 29. The Pu Distribution Near the Bottom of the Fuel Column in Element G-3. Neg. No. MSD-180624.

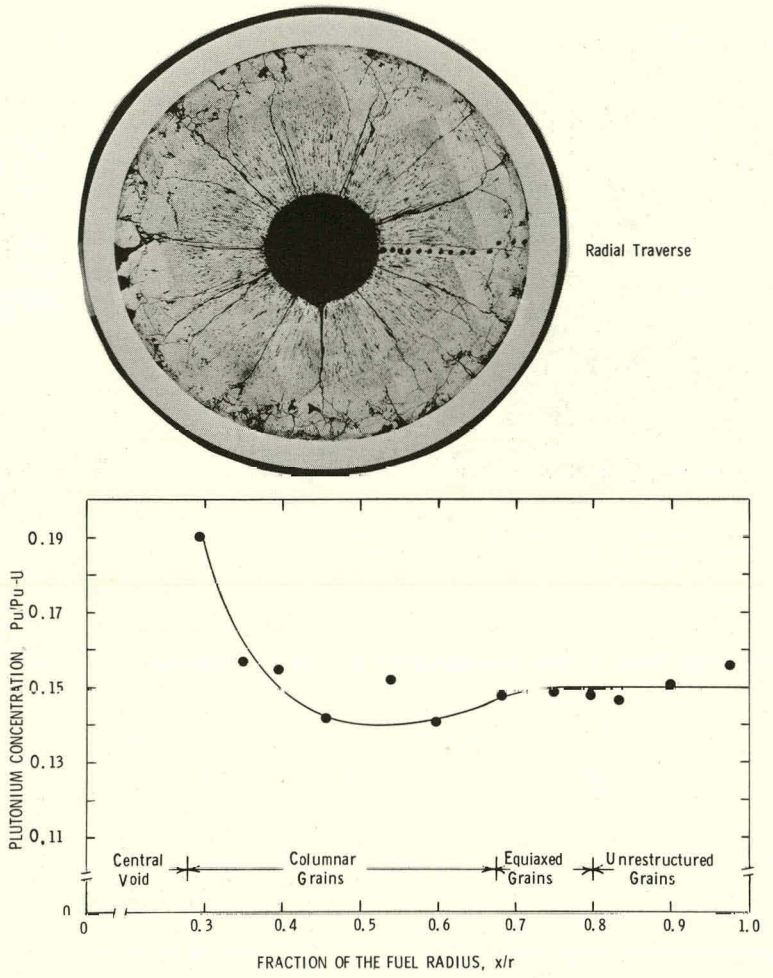

Fig. 30. Radial Pu Distribution at the Reactor-core Midplane of Element G-8. Neg. No. MSD-180622.

H. Fuel-Cladding Chemical Interaction

Cladding attack was observed in all metallographic sections cut from the element, except the bottom longitudinal section. The attack in the section 3-3/8 in. above the bottom of the fuel column was limited to a few isolated areas around the circumference of the fuel. In the other specimens (6-7/8, 10-3/4, and the top specimen), the attack was quite uniform and was present on the entire inner surface of the cladding. Optical metallography of the samples in the as-polished condition revealed that the attack extended ~0.3 mil into the cladding, as shown in Fig. 31. This depth of attack is equal to the range of fission-product recoil into the cladding. However, electron-microprobe examination has shown that the affected region in the cladding is characterized by a depletion of Cr and the presence of Cs. The results of electron-microprobe analyses on a typical area of attack near the top of the fuel column are shown in Fig. 32. These x-ray images for the cladding components, Cs, and the fuel components show that Cs has concentrated in the porous, Cr-depleted inner edge of the cladding and along the outer edge of the fuel.

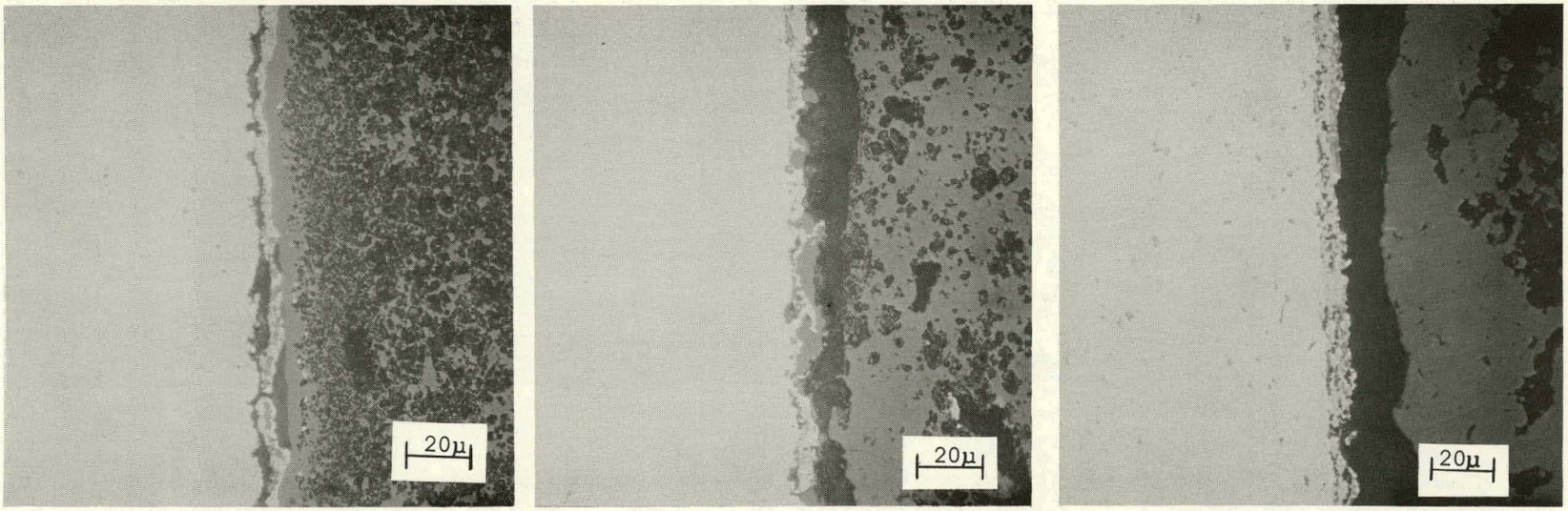

(a) (b) (c)

Fig. 31. Attack at the ID of the Cladding in Element G-3. Sample was as-polished. (a) Fuel midplane transverse section. Neg. No. MSD-164844; (b) Area 10-3/4 in. above fuel bottom transverse section. Neg. No. MSD-164848; and (c) Near top of fuel longitudinal section. Neg. No. MSD-164852.

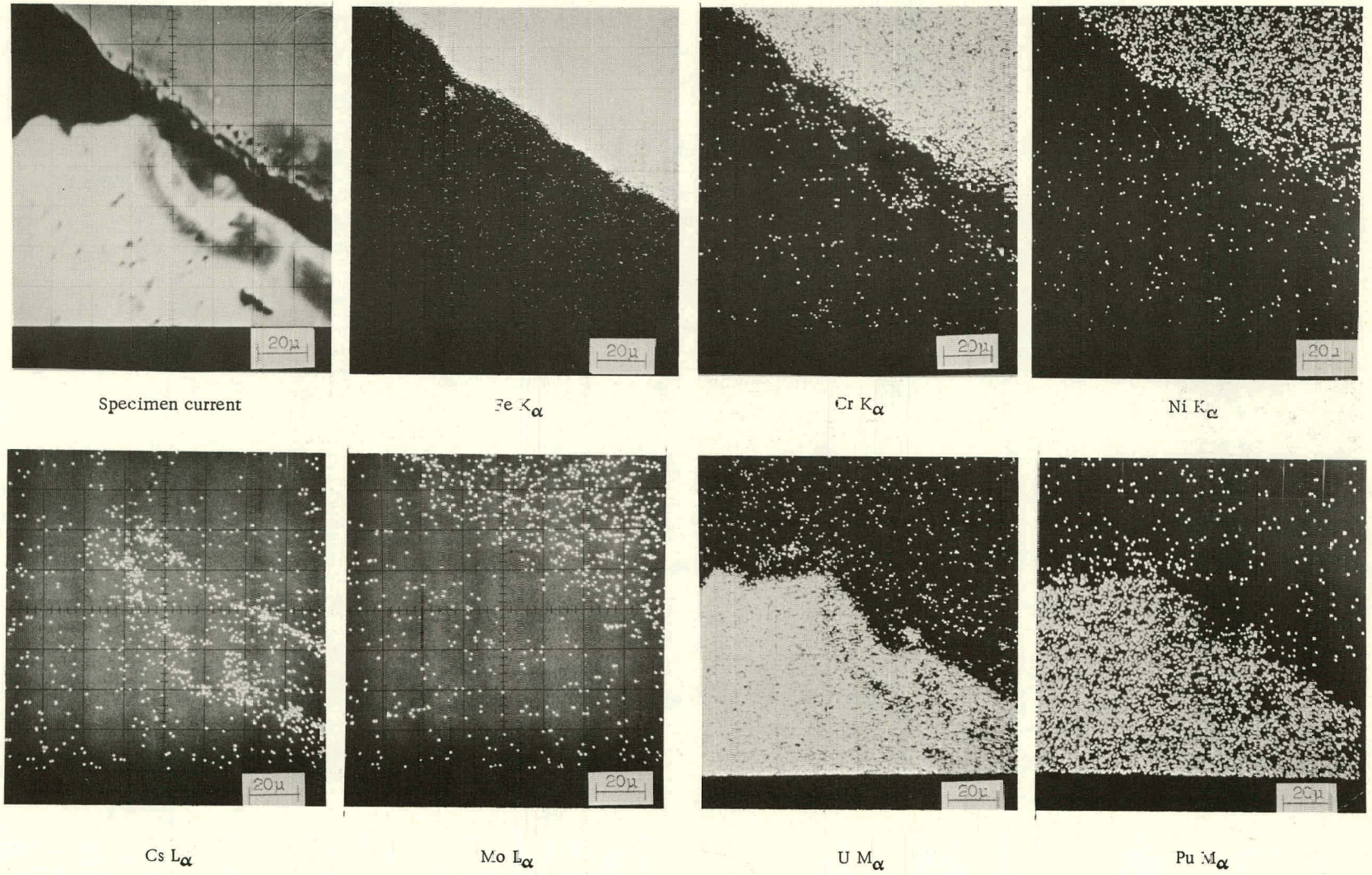

Fig. 32. Specimen Current and X-ray Images of a Typical Area of Cladding Attack Near the Top of Element C-3 Fuel Column. Neg. No. MSD-181692.

I. Cladding Microstructure

The cladding of the three transverse metallographic specimens was electro-etched with 5% HCl in methanol. The cladding microstructures are shown in Figs. 33-35. The cladding 3-3/8 in. above the bottom of the fuel column operated at ~665°C at the ID and ~625°C at the OD. The microstructure was characterized by the presence of fine carbide precipitates evenly distributed along grain boundaries and twin boundaries. At the reactor midplane, the cladding operated at ~700°C at the ID and ~660°C at the OD. The microstructure in this region was characterized by carbides in the grain and twin boundaries in the outer half of the wall thickness. Near the ID of the cladding, the precipitates coalesced into individual particles that could be resolved at a magnification of 180X. These particles were apparent throughout the entire wall thickness in the sample taken 10-3/4 in. above the bottom of the fuel column. However, they have not been positively identified, but probably are precipitates of intermetallic compounds, i.e., sigma, chi, or eta particles.

The etched structure indicates that the grain boundaries at the ID of the cladding have been altered slightly, particularly in the section 10-3/4 in. above the bottom of the fuel column. These results may indicate that fission products have migrated deeper into the grain boundaries than was apparent from the attack observed in the as-polished condition. However, it is not uncommon to observe grain boundaries at the surfaces of the cladding that are affected by sample preparation and limits of optical microscopy due to, for example, surface rounding.

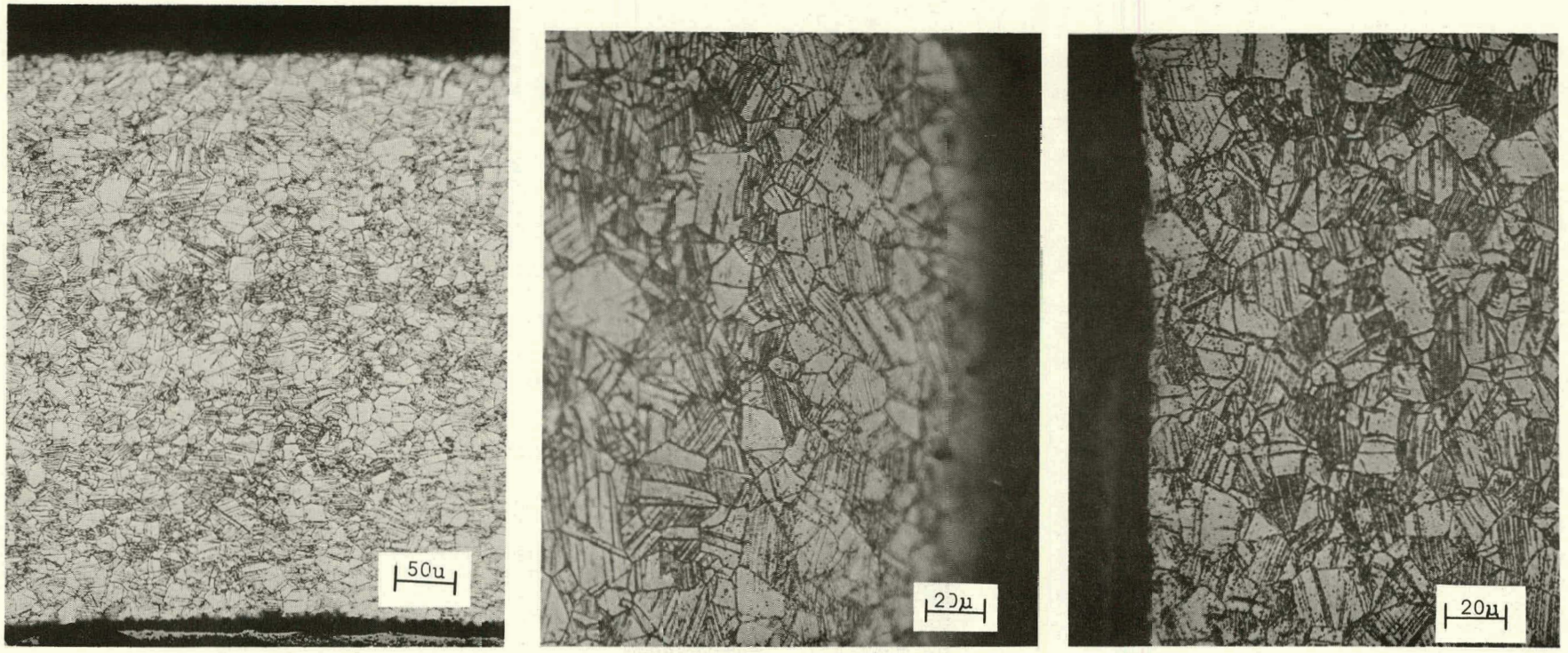

(a) (b) (c)

Fig. 33. Cladding Microstructure in the Transverse Section 3-3/8 in. above the Bottom of the Fuel Column. The sample was electroetched in 5% HCl in methanol. (a) Cladding cross section. Neg. No. MSD-164917; (b) Cladding OD. Neg. No. MSD-164919; and (c) Cladding ID. Neg. No. MSD-164918.

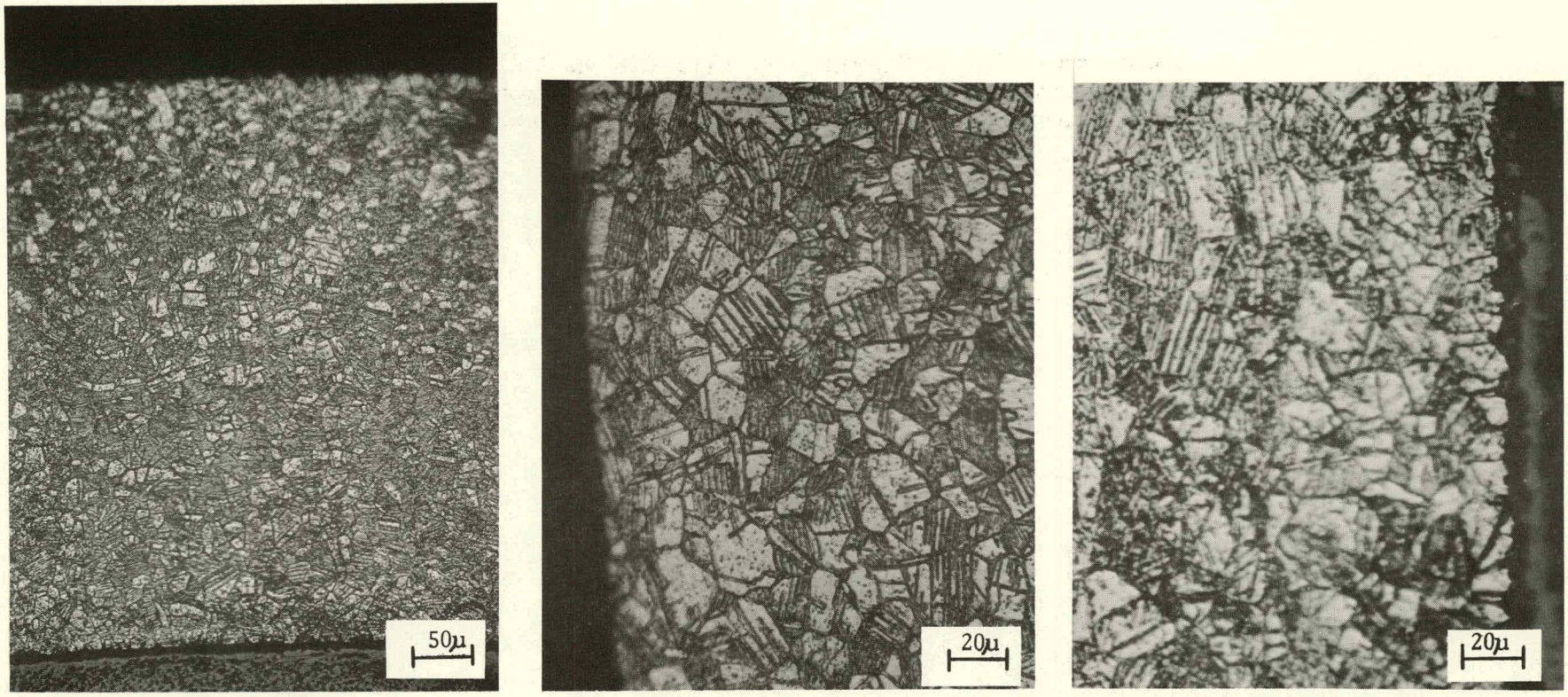

(a) (b) (c)

Fig. 34. Cladding Microstructure in the Transverse Section 6-7/8 in. above the Bottom of the Fuel Column. The sample was electroetched in 10% HCl in methanol. (a) Cladding cross section. Neg. No. MSD-169712; (b) Cladding OD. Neg. No. MSD-169715; and (c) Cladding ID. Neg. No. MSD-169713.

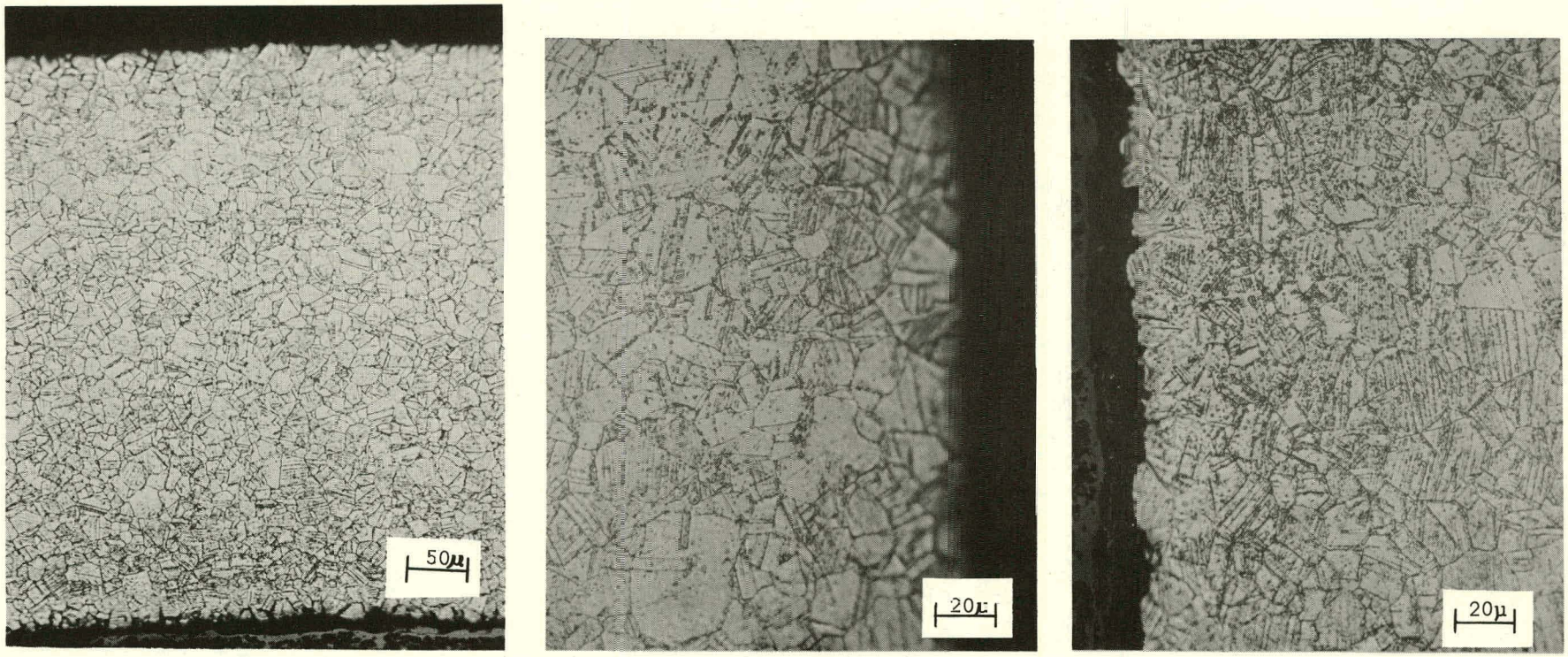

(a) (b) (c)

Fig. 35. Cladding Microstructure in the Transverse Section 10-3/4 in. above the Bottom of the Fuel Column. The sample was electroetched in 5% HCl in methanol. (a) Cladding cross section. Neg. No. MSD-164932; (b) Cladding OD. Neg. No. MSD-164934; and (c) Cladding ID. Neg. No. MSD-164933.

V. DISCUSSION OF RESULTS

The postirradiation examination of element G-3 from the F-1 series of elements revealed few unique or unusual features. One of the most striking features was the observation of fuel material that filled the hole in the annular pellets at the top and bottom of the fuel column. Electron-microprobe analyses show that the actinide distribution in the material in the central hole at the bottom of the fuel column is similar to the distribution in the typical fuel in the remainder of the element. However, the material in the central hole at the top of the fuel column had a lower Pu content and an inverted distribution, when compared with normal fuel. The Pu distribution in the fuel at the centerline near the bottom of the column was similar to the normal pellets, which may indicate the lower plug formed from fuel chips that collected at the bottom of the central void early in the life of the element. The chips may have spalled from the inner walls of the annular pellets during early power changes. The plug in the central void at the top of the fuel column may have formed by vapor deposition from the fuel. The higher vapor pressure of UO_2, in contrast to PuO_2, would then account for the reduced Pu content in this material. Additional information on the mechanism of the formation of the material in the central hole will be obtained during the examination of other elements from the F-1 series at higher burnups.

The gamma scanning showed that the volatile fission product ^{137}Cs had migrated toward the ends of the fuel column. Previous examinations[4] showed ^{131}I had a similar axial distribution and that ^{137}Cs and ^{131}I were concentrated at the OD of the fuel. Electron-microprobe analyses of sections of the element from the top, bottom, and midlength of the fuel did not indicate significant quantities of the volatile fission products. A close examination of the sectioning diagram shows that the sections examined were from areas where gamma scanning indicated low levels of ^{137}Cs. The large ^{137}Cs peak in the G-3 element was in the gap between pellets above the bottom fuel pellet. The bottom longitudinal section included only the lower portion of the bottom pellet. In all other regions of the element, it is likely that the concentrations of Cs in the fuel were below the detection limits of the electron microprobe. In fact, ^{137}Cs concentrations sufficient for detection were found only at the fuel-cladding interface in the top longitudinal section.

Another noteworthy feature observed in the G-3 was the minimal extent of cladding attack. Optical metallography and microprobe analyses showed that the depth of cladding attack was ~0.0003 in. The nominal depth for damage from fission-product recoil in stainless steel and iron is ~0.00025 in.[5,6] The electron-microprobe results show the presence of Cs and a depletion of Cr in the affected zone of the cladding, which indicates that a chemical change has occurred. A gray phase, which has the appearance of an oxide, is also present in the attack zone. These factors indicate that the affected zone in G-3 is by cladding attack rather than by fission-product recoil.

VI. CONCLUSIONS

Results of the postirradiation examinations of element G-3 showed that the element was in good condition after ~2.8 at. % burnup at peak cladding temperatures of 690°C. Diametral changes were quite small (<0.2% $\Delta D/D_0$), and the cladding attack was minor (~0.0003 in.). A potential problem area was the strong axial migration of the volatile fission products to the ends of the fuel column. A mode of fuel-element failure, as identified by Lambert et al.,[7] involves the expansion of hyperstoichiometric depleted UO_2 pellets caused by the reaction of Cs with the pellets to form Cs_2UO_4. The volume expansion causes deformation of the cladding by mechanical interaction. This is not considered to be a serious problem because the reaction can probably be prevented by adjusting the O/M of the pellets to the stoichiometric ratio or compensated for by allowing space in the element that will accommodate the expansion.

ACKNOWLEDGMENTS

The author wishes to express his gratitude to the personnel that operated the Argonne National Laboratory, Materials Science Division's Alpha-Gamma Hot-Cell Facility for the expert handling of the actual examinations on the fuel element and to J. D. B. Lambert and L. A. Neimark for their helpful discussions about the examination data.

REFERENCES

1. P. W. Flynn, R. F. Hinz, S. Langer, J. R. Lindgren, R. J. Price, T. N. Washburn, and A. F. Weinberg, "High Temperature Fast-flux Irradiation Experiment for Mixed-oxide Fuel Rods," General Atomic Co., GA-10264 (October 1970).

2. G. O. Hayner, Argonne National Laboratory (Idaho), private communication (April 1972).

3. E. R. Ebersole, Argonne National Laboratory (Idaho), private communication (May 1974).

4. S. Langer, N. L. Baldwin, J. R. Lindgren, R. V. Strain, S. Hayner, R. Bono, and L. A. Neimark, "Volatile Fission-product Migration and Platcout in CCFR Rod Irradiations," *Trans. Am. Nucl. Soc. 15* (Nov 1972).

5. J. D. B. Lambert, "Irradiation Stability of Dispersion Fuels," *Trans. Brit. Cer. Soc. 62,* 247-255 (1963).

6. H. S. Rosenbaum, J. S. Armijo, and U. E. Wolff, "Fission-fragment Damage to Type 304 Stainless Steel Fuel Cladding," General Electric Co., GEAP-5002 (Dec 1966).

7. J. D. B. Lambert, L. A. Neimark, and R. V. Strain, "A Failure Mechanism in Mixed-oxide Fuel Elements," *Trans. Am. Nucl. Soc. 17,* 193 (1973).

Distribution for ANL-76-128

Internal:

E. S. Beckjord
C. E. Till
R. Avery
L. Burris
D. W. Cissel
S. A. Davis
D. R. Ferguson
B. R. T. Frost
E. V. Krivanec
R. J. Teunis
R. S. Zeno
R. W. Weeks
F. Y. Fradin
F. A. Nichols
L. T. Lloyd
J. F. Schumar
R. B. Poeppel
T. F. Kassner
L. A. Neimark
S. Greenberg (2)
F. L. Yaggee
H. R. Thresh
A. G. Hins
D. R. Diercks
A. Purohit
K. J. Reimann
D. Stahl
D. J. Lam
N. L. Peterson
K. L. Merkle
M. B. Brodsky
H. Wiedersich
U. F. Kocks
R. W. Siegel
M. H. Mueller
W. D. Jackson
C. E. Johnson
J. E. Sanecki
J. T. Madell
R. V. Strain (15)
A. B. Krisciunas
ANL Contract File
ANL Libraries (2)
TIS Files (6)

External:

DOE-TIC, for distribution per UC-77 (165)
Manager, Chicago Operations and Regional Office, DOE
Chief, Office of Patent Counsel, DOE-CORO
Director, Technology Management, DOE-CORO
Director, DOE-RRT (2)
Chief, GCFR Branch, DOE-RRT (2)
President, Argonne Universities Association
Materials Science Division Review Committee:
- E. A. Aitken, General Electric Co., Sunnyvale
- G. S. Ansell, Rensselaer Polytechnic Inst.
- A. Arrott, Simon Fraser U.
- R. W. Balluffi, Massachusetts Inst. Technology
- S. L. Cooper, U. Wisconsin, Madison
- C. Laird, U. Pennsylvania
- M. E. Shank, Pratt & Whitney, East Hartford
- C. T. Tomizuka, U. Arizona
- A. R. C. Westwood, Martin Marietta Labs.